HHS Public Access

Author manuscript

Med Image Anal. Author manuscript; available in PMC 2018 May 01.

Published in final edited form as:

Med Image Anal. 2017 May ; 38: 215–229. doi:10.1016/j.media.2015.10.009.

On Characterizing Population Commonalities and Subject Variations in Brain Networks

Yasser Ghanbari[1], **Luke Bloy**[1,2], **Birkan Tunc**[1], **Varsha Shankar**[1], **Timothy P.L. Roberts**[2], **J. Christopher Edgar**[2], **Robert T. Schultz**[2], and **Ragini Verma**[1]

[1]Center for Biomedical Image Computing and Analytics, Department of Radiology, Perelman School of Medicine, University of Pennsylvania, Philadelphia, PA 19104

[2]Center for Autism Research, Children's Hospital of Philadelphia, Philadelphia, PA 19104

Abstract

Brain networks based on resting state connectivity as well as inter-regional anatomical pathways obtained using diffusion imaging have provided insight into pathology and development. Such work has underscored the need for methods that can extract sub-networks that can accurately capture the connectivity patterns of the underlying population while simultaneously describing the variation of sub-networks at the subject level. We have designed a multi-layer graph clustering method that extracts clusters of nodes, called ‘network hubs’, that display higher levels of connectivity within the cluster than to the rest of the brain. The method determines an atlas of network hubs that describes the population, as well as weights that characterize subjectwise variation in terms of within- and between-hub connectivity. This lowers the dimensionality of brain networks, thereby providing a representation amenable to statistical analyses. The applicability of the proposed technique is demonstrated by extracting an atlas of network hubs for a population of typically developing controls (TDCs) as well as children with autism spectrum disorder (ASD), and using the structural and functional networks of a population to determine the subject-level variation of these hubs and their inter-connectivity. These hubs are then used to compare ASD and TDCs. Our method is generalizable to any population whose connectivity (structural or functional) can be captured via non-negative network graphs.

Graphical abstract

The aim of this work is (a) to create a hub atlas for a population by mapping a collection of multi-node brain networks into a system of network hubs, and (b) given a subject's network, quantify the contribution of each network hub at the subject level (illustrated by the size of the hub) as well as the strength of the inter-connectivity between pairs of hubs in the subject's network (illustrated by the thickness of hub inter-connections)

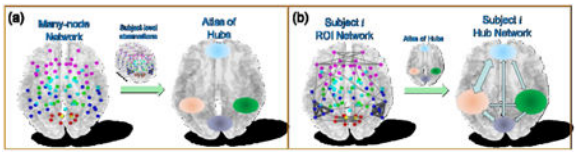

Keywords

connectivity analysis; non-negative matrix factorization; multi-layer graph clustering; population difference; autism spectrum disorder

1. Introduction

Computational techniques applied to neuro-imaging data have shown anomalies in brain activity (Ghanbari, Bloy et al. 2013) and structural connectivity (Ingalhalikar, Smith et al. 2013, Matthews, Filippini et al. 2013) in neuro-developmental disorders such as schizophrenia (Price, Cercignani et al. 2007, Skudlarski, Jagannathan et al. 2010) and autism spectrum disorder (Jou, Jackowski et al. 2011, Vissers, Cohen et al. 2012). Structural connectivity relies on diffusion imaging to characterize anatomical connections between brain regions (Mori and van Zijl 2002, Friman, Farneback et al. 2006). It is quantified using probabilistic (Behrens, Johansen-Berg et al. 2003, Behrens, Woolrich et al. 2003, Friman, Farneback et al. 2006) or streamline (Mori and Barker 1999, Mori, Crain et al. 1999, Mori and Zijl 2002) tractography performed on the diffusion imaging data, resulting in non-negative measures indicative of structural connectivity between brain regions. Functional connectivity based on fMRI, MEG or EEG is investigated at rest or during tasks by quantifying the similarity of temporal characteristics or coherence of brain activity between brain regions using methods such as correlation (Martijn and Hilleke 2010), synchronization likelihood (Barttfeld, Wicker et al. 2011, Kim, Bolbecker et al. 2013, van Dellen, Hillebrand et al. 2013), and coherence (Sakkalis 2011), or phase-amplitude coupling (PAC) (Berman, Liu et al. 2014). Such measures tell us whether there is a structural pathway or functional communication between the two regions (or with PAC connectivity in a local region as well as between regions), and the strength of the connection. While task-related functional connectivity captures brain networks associated with information processing (Sporns, Tononi et al. 2000), resting state functional connectivity facilitates the study of connectivity in the absence of external stimulation, (Mantini, Perrucci et al. 2007, Assaf, Jagannathan et al. 2010).

Autism spectrum disorder (ASD) is a developmental disorder characterized by social and communication impairments, as well as repetitive and restricted behaviors (APA 1994, APA 2000). Research indicates that many ASD symptoms are associated with abnormal structural and functional brain connectivity (Vissers, Cohen et al. 2012, Edgar, Heiken et al. 2014, Ghanbari, Smith et al. 2014). Current theories of brain connectivity in ASD primarily report local over-connectivity in the frontal regions and long range under-connectivity (Just, Keller et al. 2012, Vissers, Cohen et al. 2012). For example, MRI structural connectivity studies suggest ASD is characterized by enhanced short-range and decreased long-range connectivity (Courchesne and Pierce 2005). MRI functional connectivity studies also report

abnormalities, with atypical connectivity between brain regions reported in fMRI studies of ASD, in domains such as social interaction (Perkins, Stokes et al. 2010), face processing (Critchley, Daly et al. 2000, Schultz, Gauthier et al. 2000), as well as in other cognitive tasks (Castelli, Frith et al. 2002, Just, Cherkassky et al. 2004, Just, Cherkassky et al. 2007). Electroencephalography (EEG) and magnetoencephalography (MEG) have also examined resting-state activity in ASD, showing that brain connectivity in ASD does not fit into the small-world network model observed in controls (Barttfeld, Wicker et al. 2011), and that in ASD functional connectivity is deficient in long-range fronto-occipital connections and is excessive in short-range frontal connections (Coben, Clarke et al. 2008, Barttfeld, Wicker et al. 2011). Local occipital-parietal resting-state connectivity abnormalities have also been recently reported (Berman, Liu et al. 2014).

Given that many neurodevelopmental disorders are thought to be disorders of connectivity, the analysis of brain connectivity is of high importance. Recently, connectivity analysis has focused on representing brain connectivity using graphs, where the brain is divided into regions of interest (ROI), each of which is a node in the graph, with the edges weighted with the connection strength between two brain ROIs. Graph representations are, however, of high dimensionality, and thus difficult to analyze and interpret. Graph theory metrics (Bullmore 2009, Rubinov and Sporns 2010) have been recently introduced to analyze the complex organization of brain networks by providing features such as small-worldness, modularity, centrality, and participation coefficient (Sporns, Honey et al. 2007, Bassett, Brown et al. 2011, Ingalhalikar, Smith et al. 2013). Although some of these features have shown to be associated with pathology (Barttfeld, Wicker et al. 2011, Rudie, Brown et al. 2012, Griffa, Baumann et al. 2013), they are difficult to interpret for non-sparse and highly variable connectivity networks.

Commonalities in these networks over a population, and the variation at the individual level, underline the need for a network analysis methodology that can extract sub-networks that are able to characterize the population network structure while reducing dimensionality. Ideally, these sub-networks will describe local brain processes, with sub-network interactions measuring communication between sub-networks, thereby characterizing long- and short-range connectivity patterns. This would provide an interpretable brain network map while also facilitating statistical analyses that describe how this brain network is affected by disease. Although traditional approaches such as principal and independent components analysis (PCA and ICA) (Calhoun, Kiehl et al. 2008) provide dimensionality reduction, such approaches when applied to functional or structural connectivity networks, in the absence of positivity constraints, produce components that often lack physiological interpretability. Such positivity constraints are needed in the case of DTI-based connectivity matrices, as the connection measures quantify the anatomical connectivity between regions; hence its relationship with anatomy is the constraining factor for it to be non-negative. In functional connectivity, too, when the connectivity is quantified by a non-negative measure, like synchronization likelihood, as opposed to correlation, the components or sub-networks obtained from analysis are interpretable in the same space of connectivity quantification if they are non-negative.

Recently, hierarchical mixture model was used estimated functional networks in resting state fMRI (Liu, Awate et al. 2014). This model finds networks that account for both within subject coherence and between-subject consistency of the network label maps, however does not constrain the networks with non-negativity that is important for interpretability in applications such as MEG or DTI.

To overcome this issue, non-negative matrix factorization (NMF) and its alternatives have recently gained attention and have been effective in providing an interpretable set of bases characterizing multivariate data. Since its introduction by Lee and Seung (Lee and Seung 1999), NMF has been successfully employed in applications such as signal processing, pattern recognition, data mining, and medical imaging (Berry, Browne et al. 2007, Yang and Oja 2010, Batmanghelich, Taskar et al. 2012, Ghanbari, Smith et al. 2013). Despite the advantages in interpretability that NMF offers over other dimensionality reduction techniques (PCA, ICA, etc), due principally to its part-based representation of data and non-negativity constraints on both the bases and coefficients, it does possess drawbacks. Namely, traditional NMF requires that connectivity matrices be vectorized prior to being used as a feature vector in the analysis pipeline. This vectorization of the connectivity matrix simply treats the relationship (i.e. connectivity) between pairs of nodes as independent and overlooks the inter-dependency between the connections emanating from that node, thereby losing the graph structure that such nodes and their inter-connections form.

In this paper, we present a novel approach that extracts the underlying functional/structural sub-networks that describe the hubs of the brain connectivity network while capturing variation in the population. Our framework does not treat the connectivity between pairs of nodes as being strictly independent, but instead is based on the premise that there are a few underlying sub-networks that describe the population, with variations in these networks representative of variations in the subjects. We have therefore designed a method that extracts sets of nodes - called hubs - that communicate strongly within each set, with the collection of hubs characterizing the population. As the intra- and inter-connectivity of these hubs plays an important role in describing brain connectivity, the presented method determines the dominant network hubs that characterize commonality across subjects within a population, with connectivity between these hubs capturing the individualized variation (e.g., due to inherent heterogeneity or induced by pathology). This collection of network hubs is referred to as a network atlas. Fig. 1-left illustrates a hub atlas composed of four network hubs that are strongly connected within each hub (shown by thick connections) and with inter-connectivity between hubs shown by dashed lines.

The manifestation of the network atlas at the subject level can be highly variable (as illustrated in Fig. 1-right). Hence, the primary aim of this work is to identify the network hubs of the population, that define its atlas of connectivity. These hubs will determine the commonalities across the population networks, as illustrated in Fig. 2(a). As shown in Fig. 2(b), given the connectivity network of a subject and the atlas of hubs, our proposed method will: (a) quantify the contribution of each hub to that subject's network (illustrated by the size of each hub on the right side of Fig 2(b)), and (b) quantify the overall interaction (inter-connectivity) between pairs of hubs (illustrated by the thickness of connections between

hubs on the right side of Fig 2(b)). These subject-level measures will then be used for statistical analysis and group comparisons.

The approach we take to extract network hubs is based on multi-layer graph clustering. The advent of graph-based clustering techniques, such as spectral clustering, has led to a growing interest in methods for the clustering of multi-layer graphs in the area of mobile phone networks and document clustering (Tang, Lu et al. 2009, Dong, Frossard et al. 2012, Dong, Frossard et al. 2014). Such approaches primarily deal with multiple modalities of information, where each modality conveys one aspect of data relationship represented by a graph. These graphs then form a multi-layer graph, where each layer has the same set of nodes but with differing edge weights between nodes. However, such methods lack interpretability as they are primarily concerned with the approximation of a graph Laplacian that can be used in a spectral clustering algorithm.

While edgewise statistics of these networks can be used to determine connectivity variation in a population, their high dimensionality makes the correction of multiple comparisons as well as the interpretability of disjoint set of significantly different edges, challenging. These issues are reduced in our approach, where the brain network is split into a small number of interpretable hubs that jointly characterize the population, along with a set of weights describing their interaction, thereby making this high dimensional problem amenable to group-wise statistics.

In the proposed technique, the network matrix of each subject forms one layer of our multi-layer network graph. A matrix factorization scheme decomposes the multi-layer connectivity network into a collection of network hubs capturing the underlying connectivity shared among all network layers, as well as a set of subject-level weights representing variation of the hubs at the individual level. The decomposition scheme is constrained by the non-negativity of both the network hubs and their weights so that the hubs obtained are interpretable networks on their own, and the associated subject-level weights are representative of the magnitude of the contribution of the corresponding hub to the subject's brain network. These network hubs are extracted using a gradient descent approach, minimizing the reconstruction error of the connectivity matrix decomposition.

The applicability of the proposed method is demonstrated on TDCs and children with ASD, examining networks from resting-state MEG data as well as diffusion tensor imaging (DTI) data. For each modality, connectivity matrices of the patient and controls are stacked together to form the pooled ASD-TDC multi-layer connectivity graph. Then, using our framework, a common set of network hubs that characterizes the variability in the population, is extracted, as well as the subject-level weights that can be used for group-based statistics. Results establish the generalizability of the proposed method for the analysis of brain networks derived from any structural or functional modality.

2. Material and Methods

2.1 Participants

We demonstrate the applicability of our method in two separate analyses with different subjects using functional resting-state magnetoencephalography (MEG) data and structural white matter (DTI) data.

2.1.1 MEG data—The dataset consisted of 77 male children, 37 ASD and 40 TDCs, aged 6-14 years (mean=10.2 years, SD=1.8 in ASD, and mean=10.3 years, SD=1.7 in TDC, no significant group difference in age, $p>0.6$). Resting state MEG was acquired in a magnetically shielded room using a 306-channel Elekta scanner. Five minutes of data were recorded with sampling frequency of 1kHz, from which two minutes were retained after artifact removal and quality assurance. Data were low-pass filtered before downsampling to 500 Hz to avoid aliasing.

2.1.2 DTI data—The DTI dataset used here includes data from 116 individuals with ASD and 82 age-matched TDCs, aged 6—19 years (mean=12.7 years, SD=3.1 in ASD, and mean=12.4 years, SD=3.2 in TDC, no significant group difference in age, $p>0.5$).

DTI data was acquired on a Siemens 3T Verio™ scanner using a 32-channel head coil and a single shot spin-echo, echo-planar sequence with the following parameters: TR/TE = 11000/76 ms, b-value of 1000 s/mm2, 30 gradient directions. Eighty 2 mm contiguous axial slices of 128 × 128 matrix (FOV 256 mm) yielded 2 mm isotropic data. Quality assurance (QA) of the images was performed manually and the images with poor quality were removed, leaving 198 images with acceptable quality.

2.2. Creating brain network matrices

2.2.1 Brain networks based on functional connectivity—Resting-state eyes-closed data were band-pass filtered to focus on the alpha band (8–12 Hz). MEG data were divided into 2.5-second epochs with 50% overlap. For each epoch, MEG data were mapped into the frequency domain using a Fast Fourier Transform (FFT). A source grid (5mm isotropic resolution) was obtained by sampling cortical gray-matter areas from each subject's T1-weighted MRI. The sensor-space frequency-domain data were used as input to the frequency-domain VESTAL (Huang, Nichols et al. 2012) to obtain source amplitude (root mean squared) at each source location. From this spatial distribution of source amplitudes an inverse operator was determined (Huang, Huang et al. 2014) and applied to the MEG data to yield source time courses at each location. 301 structurally meaningful ROIs were determined using Freesurfer tools to subdivide the cortical surface of a template subject and to map these ROIs into each of the 77 subjects.

Of the 301 ROIs, 202 ROIs were identified that had at least one MEG source assigned to them. Time-courses for these 202 ROIs were determined using singular value decomposition (SVD) to extract the dominant time-course from each ROI. Connectivity matrices were then computed for the 202 regions yielding 77 matrices of size 202×202. Synchronization likelihood (SL), a non-negative measure of synchronous activity between 0 (no connection) and 1 (completely synchronous) quantified functional connectivity between two regions. In

this scheme, two brain regions were considered highly synchronous if the temporal activity pattern of one region repeats itself at certain time instants within a time period while the other region's temporal activity repeats itself at those same time instants. Mathematical details for computation of SL connectivity matrices can be found in Appendix A. Figure 3 shows the procedure of creating functional connectome from MEG signals.

2.2.2 Brain networks based on Structural connectivity—DTI data were fitted with a tensor model from which the fractional anisotropy (FA) map was computed. The high resolution T1 structural images were parcellated into 95 regions (68 cortical and 27 sub-cortical) using Desikan atlas (Desikan, Segonne et al. 2006) in Freesurfer. The 95 region labels were then transferred to the Gray matter – white matter (GM-WM) boundary (GM voxels neighboring a WM voxel) using in-house developed software and then subsequently to the diffusion space via an affine registration (T1 to FA). Probabilistic fiber tracking (Behrens, Johansen-Berg et al. 2003) was performed from each of these regions with 5000 streamline fibers sampled per voxel, resulting in a 95×95 matrix of weighted connectivity values, where each element of the matrix represents the probability of a pathway between regions, normalized by the active surface area of the seed ROI. Figure 4 demonstrates the procedure of creating a structural connectome.

2.3. Modeling Network Hubs and their Inter-connectivity

Given a group of subjects, a network atlas is created using the connectivity matrices from all subjects. Connectivity is quantified by a non-negative similarity measure between n regions, leading to a non-negative connectivity matrix of subject m, i.e. $\mathbf{S}^{(m)} \in \Re^{n\times n}$ represented by a graph with n vertices. A matrix factorization model $\mathbf{S}^{(m)} \approx \mathbf{U}\mathbf{\Lambda}^{(m)}\mathbf{U}^T$ is then used, where the columns of $\mathbf{U} = [\mathbf{u}_1, \mathbf{u}_2, \ldots, \mathbf{u}_k] \in \Re^{n\times k}$ correspond to a set of highly interconnected nodes common to the subjects and characterize the shared underlying hubs of the population. $\mathbf{\Lambda}^{(m)} = \left[\lambda_{ij}^{(m)}\right] \in \Re^{k\times k}$ is a symmetric matrix capturing the weights of each subject's network hubs, and thus providing low-dimensional representations that explain subject-level variations of the corresponding hub. $k \ll n$ is the number of network hubs to be identified. Fig. 5 shows this decomposition procedure (although the networks may not be as clean and consistent across subjects due to inter-individual variations).

Due to the symmetry of $\mathbf{\Lambda}^{(m)}$, this decomposition model can be re-written as

$$\mathbf{S}^{(m)} \approx \mathbf{U}\mathbf{\Lambda}^{(m)}\mathbf{U}^T = \sum_{i=1}^{k}\sum_{j=1}^{k}\lambda_{ij}^{(m)}\mathbf{u}_i\mathbf{u}_j^T = \sum_{i=1}^{k}\lambda_{ii}^{(m)}\mathbf{u}_i\mathbf{u}_i^T + \sum_{i=1}^{k}\sum_{\substack{j=1\\ j>i}}^{k}\lambda_{ij}^{(m)}\left(\mathbf{u}_i\mathbf{u}_j^T + \mathbf{u}_j\mathbf{u}_i^T\right). \quad (1)$$

In this model, each network hub is identified by the first term in Eq. (1), i.e. $\mathbf{u}_i\mathbf{u}_i^T \in \Re^{n\times n}$, with subject-level intra-connectivity strength within the hub, represented by the diagonal coefficients $\lambda_{ii}^{(m)}$. On the other hand, the subject-level inter-connectivity variation between hubs i and j is represented by off-diagonal coefficients $\lambda_{ij}^{(m)}\left(=\lambda_{ji}^{(m)}\right)$, with the inter-

connectivity pattern identified by $\mathbf{u}_i\mathbf{u}_j^T+\mathbf{u}_j\mathbf{u}_i^T \in \Re^{n\times n}$, as seen in the second term of Eq. (1).

Elements of **U** are constrained to remain non-negative, thus retaining the interpretation of components (i.e. $\mathbf{u}_i\mathbf{u}_j^T$) as a connectivity matrix (i.e. hubs and their inter-connectivity). $\mathbf{\Lambda}^{(m)}$ is constrained to be symmetric due to the symmetry of connectivity matrices $\mathbf{S}^{(m)}$, but it is worth noting that $\mathbf{\Lambda}^{(m)}$ is not diagonal as this allows the model to capture the inter-connectivity weights on off-diagonal elements, thereby incorporating the inter-connectivity between the network hubs.

2.3.1 Optimization model for hubs—As we want to obtain the underlying network hubs shared between all subjects in the population, connectivity graph of all subjects in the population are stacked to form a multi-layer graph$\{\mathbf{S}^{(m)}\}$. The network hubs shared by the population are then obtained by minimizing the reconstruction error of the decomposition across layers. This can be obtained by minimizing the following objective function

$$J\left(\mathbf{U},\mathbf{\Lambda}^{(m)}\right)=\sum_{m=1}^{M}\|\mathbf{S}^{(m)}-\mathbf{U}\mathbf{\Lambda}^{(m)}\mathbf{U}^T\|_F^2+\beta\left(\|\mathbf{U}\|_F^2+\sum_{m=1}^{m}\|\mathbf{\Lambda}^{(m)}\|_F^2\right),\ \text{subject to}\ \mathrm{U_{ij}}\geq 0,\lambda_{ij}^{(m)}\geq 0,\text{and}\mathbf{\Lambda}^{(m)}=\mathbf{\Lambda}^{(m)\,T} \tag{2}$$

where M is the number of subjects, and $\|\cdot\|_F$ denotes the Frobenius norm. The regularization term, as the sum of the squared norm of **U** and $\mathbf{\Lambda}^{(m)}$, is added to improve numerical stability, and β is a tunable parameter balancing the two terms of reconstruction error norm and regularization. The non-negativity constraints on **U** maintains the interpretation of network hubs as a connectivity matrix, and non-negativity of coefficients $\mathbf{\Lambda}^{(m)}$ defines them as weights of those network hubs forming the subject's overall network.

2.3.2 Computing hubs and their subject-level weights—The objective function of Eq. (2) can be rewritten as

$$J\left(\mathbf{U},\mathbf{\Lambda}^{(m)}\right)=\sum_{m=1}^{M}\mathrm{trace}\left\{\left(\mathbf{S}^{(m)}-\mathbf{U}\mathbf{\Lambda}^{(m)}\mathbf{U}^T\right)^2\right\}+\beta\left(\mathrm{trace}\{\mathbf{U}\mathbf{U}^T\}+\sum_{m=1}^{m}\mathrm{trace}\left\{\mathbf{\Lambda}^{(m)^2}\right\}\right),\ \text{subject to}\ \mathrm{U_{ij}}\geq 0,\lambda_{ij}^{(m)}\geq 0,\text{and}\mathbf{\Lambda}^{(m)}=\mathbf{\Lambda}^{(m)\,T} \tag{3}$$

To minimize Eq. (3) with respect to the non-negativity constraints, an iterative procedure is proposed with the matrices **U** and $\mathbf{\Lambda}^{(m)}$ alternately optimized by the given multi-layer graph of the population $\{\mathbf{S}^{(m)}\}$. The gradient decent approach is then used, i.e. alternately updating $\mathrm{U_{ij}}=\mathrm{U_{ij}}-\eta_{ij}\frac{\partial J}{\partial \mathrm{U_{ij}}}$ and $\lambda_{ij}^{(m)}=\lambda_{ij}^{(m)}-\xi_{ij}^{(m)}\frac{\partial J}{\partial \lambda_{ij}^{(m)}}$ with step sizes $\eta_{ij}\geq 0$ and $\xi_{ij}^{(m)}\geq 0$, where

$$\frac{\partial J}{\partial \mathbf{U}} = -4\sum_{m=1}^{M}\left[\left(\mathbf{S}^{(m)} - \mathbf{U}\boldsymbol{\Lambda}^{(m)}\mathbf{U}^{T}\right)\mathbf{U}\boldsymbol{\Lambda}^{(m)}\right] + 4\beta\mathbf{U}, \tag{4}$$

and

$$\frac{\partial J}{\partial \boldsymbol{\Lambda}^{(m)}} = -2\mathbf{U}^{T}\left(\mathbf{S}^{(m)} - \mathbf{U}\boldsymbol{\Lambda}^{(m)}\mathbf{U}^{T}\right)\mathbf{U} + 2\beta\boldsymbol{\Lambda}^{(m)}. \tag{5}$$

Due to non-negativity of connectivity matrices $\mathbf{S}^{(m)}$, our non-negativity constraints will be guaranteed by positive initialization of $\mathbf{U}$ and (symmetric) $\boldsymbol{\Lambda}^{(m)}$, and applying the step sizes

$$\eta_{ij} = \frac{\frac{1}{4}\mathrm{U}_{\mathrm{ij}}}{\left(\beta\mathbf{U} + \sum_{m=1}^{M}\mathbf{U}\boldsymbol{\Lambda}^{(m)}\mathbf{U}^{T}\mathbf{U}\boldsymbol{\Lambda}^{(m)}\right)_{ij}},\ \xi_{ij}^{(m)} = \frac{\frac{1}{2}\lambda_{ij}^{(m)}}{\left(\mathbf{U}^{T}\mathbf{U}\boldsymbol{\Lambda}^{(m)}\mathbf{U}^{T}\mathbf{U} + \beta\boldsymbol{\Lambda}^{(m)}\right)_{ij}}. \tag{6}$$

This results in the following multiplicative updating solutions

$$\mathrm{U}_{\mathrm{ij}} = \mathrm{U}_{\mathrm{ij}}\frac{\left(\sum_{m=1}^{M}\mathbf{S}^{(m)}\mathbf{U}\boldsymbol{\Lambda}^{(m)}\right)_{ij}}{\left(\beta\mathbf{U} + \sum_{m=1}^{M}\mathbf{U}\boldsymbol{\Lambda}^{(m)}\mathbf{U}^{T}\mathbf{U}\boldsymbol{\Lambda}^{(m)}\right)_{ij}}, \tag{7}$$

and

$$\lambda_{ij}^{(m)} = \lambda_{ij}^{(m)}\frac{\left(\mathbf{U}^{T}\mathbf{S}^{(m)}\mathbf{U}\right)_{ij}}{\left(\mathbf{U}^{T}\mathbf{U}\boldsymbol{\Lambda}^{(m)}\mathbf{U}^{T}\mathbf{U} + \beta\boldsymbol{\Lambda}^{(m)}\right)_{ij}}. \tag{8}$$

Starting with initial random positive elements on $\mathbf{U}$ and (symmetric) $\boldsymbol{\Lambda}^{(m)}$, the iterative procedures (7) and (8) are performed alternately until convergence. Such an initialization guarantees the non-negativity and symmetry constraints on the objective function, as can be verified from equations (7) and (8).

2.3.3 Ranking node membership in each hub—Each column of the matrix $\mathbf{U}$ (i.e. $\mathbf{u}_i$) represents a network hub whose intra-connectivity is determined by $\mathbf{u}_i\mathbf{u}_i^T$. It is important to note that each element of $\mathbf{u}_i$ in this model indicates the membership degree of the

corresponding node (in comparison to the other nodes) in that hub. Hence, elements of $\mathbf{u}_i$ determine the rank of the node membership in the i[th] hub.

2.3.4 Statistical analysis and interpretation—As explained at the beginning of section 2.3, elements of the subject-level weight matrix $\mathbf{\Lambda}^{(m)}$ represent weights of intra- and inter-connectivity of network hubs in that subject. The intra-connectivity of network hubs is represented by the diagonal elements of $\mathbf{\Lambda}^{(m)}$, i.e. $\lambda_{ii}^{(m)}$, and the inter-connectivity of hubs is represented by upper triangular elements (due to symmetry), i.e. $\lambda_{ij}^{(m)}$, *j>i*. Hence, a significant group difference at a diagonal element $\lambda_{ii}^{(m)}$ is interpreted as alteration in the communication *within* i[th] network hub, i.e. $\mathbf{u}_i\mathbf{u}_i^T$, and a group difference at a non-diagonal element $\lambda_{ij}^{(m)}$ indicates changes in the communication *between* the network hubs *i* and *j*, i.e. the inter-connectivity pattern $\mathbf{u}_i\mathbf{u}_j^T+\mathbf{u}_j\mathbf{u}_i^T$ has perhaps been altered by disease.

3. Results

The proposed method was applied to simulated data and functional connectivity matrices computed using synchronization likelihood in MEG recordings as well as structural connectivity matrices obtained from DTI probabilistic tractography.

3.1 Extraction of Hubs in Simulated Networks

In order to investigate the performance of the proposed method, we first create a network consisting of 50 nodes forming two hubs, one comprising the first 20 nodes and the second the rest of the 30 nodes. The connectivity matrix of this network is shown in Fig. 6 (a) where red and blue colors represent one and zero, respectively. This network forms our base underlying network, and its variations are simulated by adding random non-negative noise to all zero and non-zero weighted edges. The noise was sampled from a normal distribution $\mathcal{N}(0, 1.5)^2$ and the noisy images were capped between zero and one. Four variations were created whose connectivity matrices are shown in Fig. 6 (b)-(e). These four matrices represent four subject-level variations of the underlying network architecture. The hubs are then extracted by applying the proposed method to these four matrices with k=2. The resulting hubs are shown in Fig. 6 (f)-(g). It is seen that the proposed method is capable of retrieving the underlying hubs in the presence of variations.

In order to show the subject level weights in the simulated networks, we used a similar base networks as in Fig. 6(a), and correspondingly, simulated two common factors **U** of size 50×2. Then, two sets of connectivity matrices, each consisting of 40 networks representing one group, were created. These networks were created by using the same common factor **U**, but their subject level intra-connectivity weights (λ_{11}) in the first hub (top left network in Fig. 6(a)) were sampled from the normal distributions $\mathcal{N}(5, 1^2)$ and $\mathcal{N}(6, 1^2)$, respectively, for the simulated groups 1 and 2. The different normal distributions simulate statistical group difference between weights, with group 1 having statistically lower weights. Also, intra-connectivity weights (λ_{22}) of the second hub (bottom right network in Fig. 6(b)) were randomly sampled from the normal distributions $\mathcal{N}(6, 1^2)$ and $\mathcal{N}(5, 1^2)$ or the groups 1 and

2, respectively (group 1 having statistically higher weights). The inter-connectivity weights (λ_{12}) were sampled from the same normal distribution $\mathcal{N}(0.5, 1^2)$ or both groups (no group difference), with negative numbers truncated to zero to maintain non-negativity. The subject level matrices were then constructed by $\mathbf{S}^{(m)} = \mathbf{U}\mathbf{\Lambda}^{(m)}\mathbf{U}^T + \boldsymbol{\varepsilon}^{(m)}$ where $\boldsymbol{\varepsilon}$ represents the background noise that was sampled from $\mathcal{N}(1, 0.1^2)$, and the intra- and inter-connectivity weights ($\mathbf{\Lambda}^{(m)}$) were randomly generated from the normal distributions described. The hubs and their weights were then obtained by applying the proposed model. The original and computed intra- and inter-connectivity weights of the two hubs are plotted in Fig. 7. It should be noted that the computed values were rescaled by their magnitude for comparison with the original values, as the model given by Eq. (1) is not scale-invariant between hubs and their weights. It is observed that the computed values follow the original ones with a good proximity, and the group differences are preserved as well.

The same experiment was performed with different values of the parameter beta to investigate the influence on statistical group difference of the computed weights. The t-values of group 1 vs. group 2 were obtained for three choices of parameter beta=0.01, 0.1, and 1, and the results are shown in Table 1. It is seen that statistical group differences are maintained.

In order to investigate the effect of the density of the underlying connectivity hubs as well as the magnitude of the noise, we used the same experiment, but varied the size of the underlying hubs as well as the noise variance. The density of underlying connections was changed to be 2, 8, 18, 32, and 50 percent of the overall connectivity matrix, corresponding to two blocks of size 5×5, 10×10, 15×15, 20×20, and 25×25, respectively. To control the noise variance, a coefficient c was used to scale the normal distribution standard deviations in intra-and inter-connectivity values as well as the background noise, i.e. $\mathcal{N}(\mu, (c\sigma)^2)$. This coefficient basically scales the standard deviation of the normal distributions by 10 values of c=0.5, 1, 1.5, …, 5. For each connectivity density and noise variance, 80 connectivity matrices were simulated, for which the subject-level intra- and inter-connectivity weights were computed by the proposed procedure. The mean squared error (MSE) of the rescaled computed weights were measured and plotted in Fig. 8. It is observed that sparsity of the underlying connectivity (smaller values on the vertical axes) increases the accuracy (blue colors) of the computed weights. Also higher noise variance (larger values on the horizontal axes) results in less accurate (red color) computation of weights. Also, it is observed that the accuracy of inter-connectivity weights is more sensitive to both sparsity and noise variance when compared to the computed intra-connectivity weights.

3.2 Extracting Hubs from Resting-state MEG Functional Connectivity

Connectivity matrices were derived from the MEG data of the 77 subjects described in section 2.2.1. Patients and control connectivity matrices were used to extract network hubs as well as the weight matrices corresponding to each subject (see Section 2.3.2). We set β=0.1 and used k=10 to obtain 10 network hubs and to compute the subject-level weights ($\mathbf{\Lambda}^{(m)}$). On convergence, the iterative procedure of (7) and (8) produced a common factor $\mathbf{U}$ of size 202×10 as well as 77 subject-level weight matrices $\mathbf{\Lambda}^{(m)}$ each of size 10×10. The ten resulting network hubs (i.e. the first term in equation (1), $\mathbf{u}_i\mathbf{u}_i^T$ for 1≤i≤10) are shown in Fig.

9, thresholded using a binary threshold to visualize the dominant edges (with a threshold of 0.1).

Table 2 lists the brain regions that contribute most to the 10 network hubs. As explained in section 2.3.3, the n elements of $\mathbf{u}_j$ determine the membership degree of n nodes (ROIs) in that hub. The top ranked regions are listed in Table 2.

The subject-level weights, $\mathbf{\Lambda}^{(m)}$ $1 \leq m \leq M$, were then used for group comparison. T-tests were performed on the 10 diagonal and 45 off-diagonal upper-triangular elements of $\mathbf{\Lambda}^{(m)}$. The diagonal and off-diagonal elements represent intra- and inter-connectivity within and between the network hubs, respectively. Analysis showed group differences in one of the diagonal elements, corresponding to network hub #9 ($p<0.05$). Statistical test of the off-diagonal upper-triangular elements showed group differences in five inter-hub connections. Fig. 10 shows the intra- and inter-connectivity patterns for those weights that show group difference, by displaying the intra- and inter-connectivity map generated by the first $(\mathbf{u}_i\mathbf{u}_i^T)$ and second term $(\mathbf{u}_i\mathbf{u}_j^T + \mathbf{u}_j\mathbf{u}_i^T)$ of equation (1). Patterns whose corresponding weights (λ_{ij}) are significantly lower in ASD are shown in blue (Fig. 10, a and b); while significantly higher weights in ASD are shown in orange (Fig. 10, c to f).

As mentioned above, group comparisons based on the diagonal elements revealed group differences in hub #9, displayed in Fig. 10 (c). This network hub is comprised primarily of superior frontal regions. Higher weights in ASD indicate frontal lobe hyperconnectivity, or enhanced short-range connections, an observation consistent with frontal lobe overconnectivity in ASD (Kana, Libero et al. 2011). In ASD, hyperconnectivity in hub #9 in the frontal regions coincided with hypoconnectivity between hub #9 and two distant hubs bilaterally (left hemisphere cyan hub #2 and right hemisphere turquoise hub #3), as seen in Fig. 10(a)-(b). Such decrease in fronto-parietal connections in ASD, between hub #9 and hub #2 as well as hub #9 and hub #3, are indicative of long-range underconnectivity in ASD. Additionally, ASD subjects showed increased connectivity in short-range connections between mid-central (mainly posterior cingulate) and central-right (right pre/postcentral) brain areas (i.e. hub #3 and hub #8 shown in Fig. 10(d)). Our analysis showed that, in ASD, this connection is correlated with scores on the social communication questionnaire (SCQ; $r=+0.30$, $p<0.05$). Fig. 10(e) shows that inter-connectivity between the frontal (medial-orbito frontal) and temporal/subcortical (fusiform and cerebellum) regions (i.e. hub #5 and hub #6). It is interesting that the two most significant connections ($p < 0.01$) have the right parietal hub (hub #3) in common, as shown in Fig. 10 (b) and (d). Fig. 10 (f) shows increased inter-connectivity between hubs #7 and #10. This pathway consists primarily of connections between precuneus and medial orbito-frontal regions.

Developmental differences between ASD and TDC with respect to intra- and inter-hub connectivity were examined. We used a generalized linear model (GLM) to study developmental differences, with group, age and their interaction as predictors, to regress each intra- and inter-connectivity weight across subjects. The interaction of age and group in the GLM captures differences between the trajectories of the two groups with respect to age (i.e. development). Developmental differences were observed in the inter-connectivity

between hub #5 and hub #8 ($p<0.05$), as well as in the intra-connectivity of hub #10 ($p<0.01$). The age correlation of the inter-connectivity between hubs #5 and #8 was r=-0.26 in ASD and r=+0.28 in TDC. Analysis showed that inter-connectivity between hub #5 and hub #8 primarily consists of connections of left fusiform and cerebellum with left posterior cingulate and paracenral regions. The intra-connectivity of hub #10 showed an age correlation of r=-0.29 in ASD and r=+0.35 in TDC. Hub #10 primarily consists of connections between caudal anterior cingulate and superior frontal regions. Table 3 summarizes the developmental differences observed.

3.3 Extracting Hubs from Structural Connectivity Data

The 95×95 connectivity matrices were computed from the 198 subjects using the method described in 2.2.2. These matrices were stacked and network hubs and their subject-level intra-and inter-connectivity weights were extracted using the method described in Section 2.3.2 using the same settings as used for MEG connectivity analysis(β=0.1 and k=10) to obtain 10 network hubs. On convergence, the iterative procedure of (7) and (8) produced a common non-negative factor $\mathbf{U}$ of size 95×10, as well as 198 subject-level weights $\mathbf{\Lambda}^{(m)}$ each of size 10×10. The resulting ten network hubs (i.e. the first term in equation (1), $\mathbf{u}_i\mathbf{u}_i^T$ for $1\leq i\leq 10$) are shown in Fig. 11.

As explained in section 2.3.3, nodes that contribute most to each hub were determined by their magnitude in the hub vector, and listed in Table 4.

Subject-level weights were used for group comparisons. Of the 10 diagonal and 45 upper-triangular elements, one intra- and two inter-connectivity elements were found to be significantly different (see Fig. 12).

The intra-connectivity in hub #5, shown in Fig. 12 (a), primarily consists of inter-regional connections between left insula, putamen, and caudate. The regions of dorsal striatum (putamen and caudate) are among the components of basal ganglia that are major subcortical targets within the fronto-striatal behavior control loops, as well as are parts of the reward circuitry (Kohls, Yerys et al. 2014, Ikemoto 2010). Decreased connectivity between regions related to reward processing is consistent with the recent theories of ASD that posit the idea that social motivation deficits play a central role in ASD (Chevallier, Kohls et al. 2012, Kohls, Schulte-Ruther et al. 2013). The inter-connectivity between hub #2 and hub #7 shown in Fig. 12 (b) is primarily between left middle temporal, superior parietal, and inferior temporal regions. Inter-connectivity between hub #6 and hub #9 (Fig. 12 (c)) is primarily made up of precuneus (both left and right), and inferior parietal (both left and right), left cuneus, and right post-central regions. Increased connectivity between these hubs is consistent with previous findings of increased gray matter volume (Brieber, Neufang et al. 2007) and increased functional activation (Gomot, Belmonte et al. 2008) in inferior parietal lobule. Cuneus and post-central regions are traditionally associated with visual and motor functions. The structural abnormalities in all these regions may correspond to attentional deficits and narrow interests observed in ASD.

5. Discussion

We have proposed a framework to extract brain connectivity sub-networks that are highly inter-connected and represent the hubs of brain networks that describe the population. This technique yields a set of inter-connected nodes as hubs of the network, as well as their contribution towards reconstructing subject-level networks. In addition, our model quantifies the inter-connectivity between these hubs producing subject-level connectivity weights between the hubs.

An important advantage of the proposed method is that, in contrast to other matrix factorization techniques such as PCA and ICA, the hub sub-networks are constrained to be non-negative and hence can be directly interpreted as *connectivity* sub-networks, and their intra- and inter-connectivity coefficients, as sub-network weights for each subject. For example, DTI structural connectomes are non-negative by definition, as they are meant to represent the amount of structural connections between two regions. If PCA or ICA is used to extract components, these components would not be interpretable as DTI structural connectomes due to the possibility of obtaining negative components and coefficients, as a negative connectivity would indicate a negative contribution to the anatomical substrate.

We applied our method to a set of functional connectivity networks obtained using synchronization likelihood. Fig. 9 shows that the method described here extracted hubs composed of spatially co-localized cortical regions while also being sparsely distributed over the brain. Some of these network hubs may have captured the fMRI default mode network (DMN). Specifically, the precuneus, an integral region of DMN (Cavanna 2007), was captured in both hemispheres in hub #7 as well as hub #4 (as reported in Table 2). This region is involved in self consciousness (Kjaer, Nowak et al. 2002, Lou, Luber et al. 2004) and proposed as part of a small-word network hub between parietal and prefrontal regions (Bullmore 2009). Moreover, the posterior cingulate, a central DMN node (Leech and Sharp 2014), was captured by hub #8. This region is involved in awareness and memory retrieval (Maddock, Garrett et al. 2001, Nielsen, Balslev et al. 2005), as well as visual attention (Leech and Sharp 2014). The hub #2 superior parietal region has also been shown to be a part of the DMN (Damoiseaux, Rombouts et al. 2006).

It has recently been hypothesized that autism is characterized by local over-connectivity and long-range under-connectivity (Kana, Libero et al. 2011, Wass 2011, Vissers, Cohen et al. 2012). Present observations are consistent with this hypotheses that whereas the ASD brain shows frontal to posterior long-distance under-connectivity, it shows superior frontal region connectivity, perhaps to compensate for the long-distance under-connectivity (Kana, Libero et al. 2011).

The short-range over-connectivity in superior frontal regions in ASD was observed in hub #9. Frontal over-connectivty has been hypothesized to be due to an excess of frontal neurons, diluting the impact of signals from distant brain regions and hence impeding long-range communications (Courchesne, Pierce et al. 2007).

Analyses showed fronto-parietal under-connectivity in ASD, primarily between superior frontal and bilateral parietal areas, as shown between the frontal hub #9 and parietal hubs #2

and #3 (Fig. 10 (a) and (b)). Abnormal fronto-parietal connectivity has been reported in studies investigating resting brain connectivity using fMRI (Cherkassky, Kana et al. 2006, Assaf, Jagannathan et al. 2010, Weng, Wiggins et al. 2010, Just, Keller et al. 2012), and also in EEG alpha synchronization (Murias, Webb et al. 2007, Coben, Clarke et al. 2008). Reduced fronto-posterior connectivity has also been shown in ASD studies of language (Just, Cherkassky et al. 2004), visuo-spatial processing (Damarla, Keller et al. 2010), executive function (Just, Cherkassky et al. 2007), and social processing (Schipul, Williams et al. 2012).

Present analyses showed a correlation between age and inter-connectivity between hub #3 and hub #9 (Fig. 10(b)) in TDCs. Inter-connectivity between frontal and right parietal increased with age in TDC ($r=+0.32$, $p<0.05$) and decreased with age in ASD ($r=+0.13$, $p>0.05$). This indicates that this sub-network underconnectivity becomes more pronounced in ASD, as a function of age.

In this analysis, we pooled both patient and control groups because performing analysis on the pooled ASD and TDC populations yields a common set of network hubs and their associated subject-level weights, facilitating statistical group comparison. Obtaining components separately from the two populations yields coefficients that are statistically incomparable as they do not share the same mapping space, causing spurious group differences. Moreover, pooling the patient and control groups will provide the between-group variability in the data that will be captured by the hubs.

A major concern with statistical analysis of brain networks is the problem of multiple comparisons. Although more nodes are preferred to better capture details in the connectivity analysis, more nodes significantly add to the number of network edges, and consequently the number of comparisons in statistical analyses. Although techniques are available for multiple comparison correction including Bonferroni correction (Dunn 1961), FDR (Benjamini and Hochberg 1995, Genovese, Lazar et al. 2002), and extreme statistics (Blair and Karniski 1993), analysis of brain connectivity with multiple comparison correction remains challenging (Cheol, Sang et al. 2013). The proposed method significantly reduces the number of multiple comparisons owing to the dimensionality reduction obtained by finding hubs and quantifying their intra-and inter-connectivity weights. For instance, our functional connectivity matrices of size 202×202 would typically require 20301 comparisons. Our method can reduce the number of comparisons to 55 when k=10.

The parameter beta β is a regularization term balancing the two terms of equation (2), the first being the reconstruction error term and the second is the magnitude of the hubs $\mathbf{U}$ and their weights $\mathbf{\Lambda}^{(m)}$. This parameter setting is data dependent. When β is set to a large number, the minimization of the objective function will emphasize more on minimizing the second term hence the reconstruction error (first term) will become large, and consequently the obtained hubs and their coefficients will not be a good representative of the population. On the other hand, if β is set to a very small number, the objective function will be dominated by the reconstruction error, causing instability in the resulting hubs and their coefficients during the iterative process because the regularization term that controls the magnitude change between U and $\mathbf{\Lambda}^{(m)}$ will not be influential. Our analyses on the MEG

dataset show that similar hubs are obtained with β =0.01, 0.1, 0.2. However, a value of β =1 is too large for the iterative procedure to converge in this dataset. On the other hand, very small β such as 1e-5 will change the objective to focus more on the minimization of the reconstruction error needing the hence the procedure to perform more iterations to satisfy the objective. Fig. 13 demonstrates the resulting hubs from the matrices of TDCs in the MEG dataset with three values of beta that have been experimented.

Similar experiment was performed on the DTI dataset for the 82 TDC subjects, and the hubs obtained with β=0.01, 0.1, 1 are shown in Fig. 14.

The number of hubs, K, is also dataset dependent that could be set by trying several values and optimizing a particular objective that is the interest of the application. Also, prior knowledge of neuroanatomy may be helpful in defining the number of hubs for certain cases.

To show how the hubs may change when a subset of the data is used, we applied our method to several subsets of the TDCs matrices in the MEG dataset. In this scheme, we started by extracting hubs from all the 40 subjects and then reducing them to 37, 34, 25, 15, and 5 subjects. The resulting hubs are shown in Fig. 15 below. It ican be seen that the hubs location remains mostly consistent when more than half of the subjects are used. With the number of subjects reducing to below half, changes in hubs are observed.

Similarly, the 10 hubs extracted from the structural networks of the TDC subjects are shown in Fig. 16, below. The number of subjects used in this experiment was 82 that was reduced to 60, 40, 20, 10, and 5, for which the resulting hubs are shown in Fig. 16 (a)-(f). It is observed that the consistency of the hubs is less than the MEG dataset used in this paper when number of subjects diminishes.

An additional advantage of our method is that it facilitates the modeling of brain networks into locally highly connected hubs. Such a network representation helps disambiguate the definition of short-range and long-range connections in terms of the intra- and inter-connectivity of network hubs, a strategy useful for clinical studies (Khan, Gramfort et al. 2013) but currently not well-defined. The small number of hubs in the model also helps interpret differences observed in the patient population.

Community detection methods that use betweenness centrality provide the modules in the network, which can be considered to be similar to what we find. However, these community detection methods do not provide a characterization and quantification of the modules at the subject level. Our method finds sub-networks that are common across the networks of a population and characterizes and quantifies intra- and inter-connectivity between these subnetworks at the subject level, that is lacking in community detection techniques.

The procedure introduced in this paper is also capable of assigning intra- and inter-connectivity weights to any new incoming subject after an atlas of hubs is created. This is useful if the proposed framework is to be used in a train-test scheme. After the network hubs (represented by the matrix **U**) are obtained from a set of given connectivity networks, equation (2) can be optimized, given the atlas (i.e. **U**), to obtain the weight matrix $\mathbf{\Lambda}^{(m)}$ for

the new subject. This is achieved by performing the iterative procedure (described in Eq.(8)) with non-negative random symmetric initialization of $\Lambda^{(m)}$ for the new subject, yielding the intra- and inter-connectivity weights.

The computational cost of the proposed method depends on the number of matrices in the dataset, number of nodes in each network, number of hubs (k), and the regularization parameter beta. The number of iterations depends not only on the above parameters, but also the stopping criteria of the iterative procedure. For the experiments in this paper, we used a maximum iteration of 10000, and the rate of change in the objective function to be less than 1e-5 to stop the iterations.

The proposed method is generalizable to any non-negative connectivity matrix set, as long as connectivity is interpretable when it is measured with a non-negative number. We have shown its application in the analysis of MEG-based functional as well as DTI-based structural networks. This was shown in the study of autism via an interpretable dimensionality reduction of brain networks amenable to statistical analysis. In fMRI applications, this method is applicable if connectivity is modeled by non-negative measures, e.g. when connectivity is obtained by synchronization likelihood (Sanz-Arigita, Schoonheim et al. 2010), as opposed to correlation that could be negative. Even if correlation or covariance measures are used to quantify the connectivity in fMRI, a positive contribution of the networks is needed (i.e. positivity constraints are needed for the coefficients). Then the same model / objective could be used with a different solution that requires non-negativity only on the coefficients but allows negativity on the hubs.

Our current model is generative and thus can be extended to a reconstructive-discriminative or reconstructive-regressive model of network hubs that could be used in classification or regression analyses.

6. Conclusions

We have presented a new technique for the analysis of brain networks using a low-rank matrix factorization model that extracts a set of population-specific network hubs, as well as a subject-level weight matrix capturing individualized variability, facilitating subsequent statistics. Our approach enables us to identify neurophysiological/neuroanatomical network hubs and characterize their inter-connections, thereby providing a global view of brain functional processes and structural pathways, as well as an insight into how the network is affected by disease. Application to MEG as well as DTI datasets provided a set of network hubs and their subject-level intra- and inter-connectivity weights for each dataset. Group-wise analysis of intra-and inter-connectivity weights revealed significant long-range connectivity deficiencies, as well as short-range overconnectivity in ASD. The proposed framework can be extended to any non-negative connectivity matrix, and the weights obtained in the process can be exploited for classification or regression analysis.

Acknowledgments

This research was supported by the following grants from National Institutes of Health: MH092862 and MH098010 (PI: Ragini Verma), and grants from the Pennsylvania Department of Health: SAP # 4100042728 and SAP # 4100047863 (PI: Robert T. Schultz).

Appendix A

Synchronization Likelihood

The time-frequency synchronization likelihood technique assumes that two signals are synchronized if a pattern of one signal repeats itself at certain time instants for a number of times within a certain period and another pattern in the other signal repeats itself at those same time instants (Montez, Linkenkaer-Hansen et al. 2006).

For a given signal at channel k, i.e. $x_k(t)$, the signal pattern at any given time instant t_i can be represented by an embedding vector $\mathbf{x}_{k,t_i} = \lfloor x_k(t_i), x_k(t_{i+l} + T), \ldots, x_k(t_{i+(m-1)l}) \rfloor$ where l is the lag and m is the length of the embedding vector. l and m are typically set to $l = \frac{f_s}{3h_f}$ and $m = \frac{3h_f}{l_f} + 1$ where f_s is the sampling frequency, and h_f and l_f are the high and low frequency contents of the signal, respectively. At each time instant t_i, the Euclidean distance is then measured between the reference embedding vector $\mathbf{x}_{k,\ t_i}$ and the set of all other embedding vectors at times t_j, i.e. $\mathbf{x}_k$ where $\mathbf{t}_j$ lies in the range $t_i - \frac{t_{w_2}}{2} < t_j < t_i - \frac{t_{w_1}}{2}$ or $t_i - \frac{t_{w_1}}{2} < t_j < t_i + \frac{t_{w_2}}{2}$ where $t_{w_1} = \frac{2l(m-1)}{f_s}$ and $t_{w1} < t_{w2}$. Then, n_{ref} nearest embedding vectors $\mathbf{x}_{k,t_j}$ are retained. This procedure is conducted for each channel k and each time instant t_i. The SL between channel k_1 and channel k_2 at time instant t_i is the number of simultaneous embedding vector recurrences in the two channels divided by the total number of recurrences, i.e. $SL_{t_i} = \frac{n_{k_1 k_2}}{n_{\text{ref}}}$. Fig. 17 illustrates how SL is calculated.

References

Alexander AL, Lee JE, Lazar M, Boudos R, DuBray MB, Oakes TR, Miller JN, Lu J, Jeong EK, McMahon WM, Bigler ED, Lainhart JE. Diffusion tensor imaging of the corpus callosum in Autism. Neuroimage. 2007; 34(1):61–73. [PubMed: 17023185]

APA. Diagnostic and statistical manual of mental disorders: DSM-IV. Washington, DC: American Psychiatric Press; 1994.

APA. DSM-IV-TR, Diagnostic and Statistical Manual of Mental Disorders. 4th., text revision. Washington, DC: American Psychiatric Association; 2000.

Assaf M, Jagannathan K, Calhoun VD, Miller L, Stevens MC, Sahl R, O'Boyle JG, Schultz RT, Pearlson GD. Abnormal functional connectivity of default mode sub-networks in autism spectrum disorder patients. Neuroimage. 2010; 53(1):247–256. [PubMed: 20621638]

Barttfeld P, Wicker B, Cukier S, Navarta S, Lew S, Sigman M. A big-world network in ASD: dynamical connectivity analysis reflects a deficit in long-range connections and an excess of short-range connections. Neuropsychologia. 2011; 49(2):254–263. [PubMed: 21110988]

Bassett DS, Brown JA, Deshpande V, Carlson JM, Grafton ST. Conserved and variable architecture of human white matter connectivity. Neuroimage. 2011; 54(2):1262–1279. [PubMed: 20850551]

Batmanghelich NK, Taskar B, Davatzikos C. Generative-Discriminative Basis Learning for Medical Imaging. IEEE Transactions on Medical Imaging. 2012; 31(1):51–69. [PubMed: 21791408]

Behrens TE, Johansen-Berg H, Woolrich MW, Smith SM, Wheeler-Kingshott CA, Boulby PA, Barker GJ, Sillery EL, Sheehan K, Ciccarelli O, Thompson AJ, Brady JM, Matthews PM. Non-invasive mapping of connections between human thalamus and cortex using diffusion imaging. Nat Neurosci. 2003; 6(7):750–757. [PubMed: 12808459]

Behrens TE, Woolrich MW, Jenkinson M, Johansen-Berg H, Nunes RG, Clare S, Matthews PM, Brady JM, Smith SM. Characterization and propagation of uncertainty in diffusion-weighted MR imaging. Magn Reson Med. 2003; 50(5):1077–1088. [PubMed: 14587019]

Benjamini Y, Hochberg Y. Controlling the false discovery rate: a practical and powerful approach to multiple testing. J R Stat Soc Series B Stat Methodol. 1995:289–300.

Berman JI, Liu S, Bloy L, Blaskey L, Roberts TPL, Edgar JC. Alpha-to-Gamma Phase-amplitude Coupling Methods and Application to Autism Spectrum Disorder. Brain Connectivity. 2014 In press.

Berry MW, Browne M, Langville AN, Pauca VP, Plemmons RJ. Algorithms and applications for approximate nonnegative matrix factorization. Computational Statistics. 2007; 52:155–173.

Blair RC, Karniski W. An alternative method for significance testing of waveform difference potentials. Psychophysiology. 1993; 30:518–524. [PubMed: 8416078]

Brieber S, Neufang S, Bruning N, Kamp-Becker I, Remschmidt H, Herpertz-Dahlmann B, et al. Konrad K. Structural Brain Abnormalities In Adolescents With Autism Spectrum Disorder And Patients With Attention Deficit/hyperactivity Disorder. Journal of Child Psychology and Psychiatry. 2007; 48(12):1251–1258. [PubMed: 18093031]

Bullmore, Ea, S, O. Complex brain networks: graph theoretical analysis of structural and functional systems. Nat Rev Neurosci. 2009; 10(3):186–198. [PubMed: 19190637]

Calhoun V, Kiehl K, Pearlson G. Modulation of temporally coherent brain networks estimated using ica at rest and during cognitive tasks. Human Brain Mapping. 2008; 29(7):828–838. [PubMed: 18438867]

Castelli F, Frith C, Happe F, Frith U. Autism, Asperger Syndrome and brain mechanisms for the attribution of mental states to animated shapes. Brain. 2002; 125:1839–1849. [PubMed: 12135974]

Cavanna AE. The precuneus and consciousness. CNS Spectr. 2007; 12(7):545–552. [PubMed: 17603406]

Cheol EH, Sang WY, Sang WS, Duk LN, Joon-Kyung S. Cluster-Based Statistics for Brain Connectivity in Correlation with Behavioral Measures. PLoS one. 2013; 8(8):e72332. [PubMed: 23977281]

Cherkassky VL, Kana RK, Keller TA, Just MA. Functional connectivity in a baseline resting-state network in autism. Neuroreport. 2006; 17(16):1687–1690. [PubMed: 17047454]

Chevallier C, Kohls G, Troiani V, Brodkin E, Schultz R. The social motivation theory of autism. Trends in Cognitive Sciences. 2012; 16(4):231–239. [PubMed: 22425667]

Coben R, Clarke AR, Hudspeth W, Barry RJ. EEG power and coherence in autistic spectrum disorder. Clin Neurophysiol. 2008; 119(5):1002–1009. [PubMed: 18331812]

Courchesne E, Pierce K. Why the frontal cortex in autism might be talking only to itself: local over-connectivity but long-distance disconnection. Current Opinion in Neurobiology. 2005; 15(2):225–230. [PubMed: 15831407]

Courchesne E, Pierce K, Schumann CM, Redcay E, Buckwalter JA, Kennedy DP, Morgan J. Mapping early brain development in autism. Neuron. 2007; 56(2):399–413. [PubMed: 17964254]

Critchley HD, Daly EM, Bullmore ET, Williams SC, Van Amelsvoort T, Robertson DM, Rowe A, Phillips M, McAlonan G, Howlin P, Murphy DG. The functional neuroanatomy of social behaviour: changes in cerebral blood flow when people with autistic disorder process facial expressions. Brain. 2000; 123(Pt 11):2203–2212. [PubMed: 11050021]

Damarla SR, Keller TA, Kana RK, Cherkassky VL, Williams DL, Minshew NJ, Just MA. Cortical underconnectivity coupled with preserved visuospatial cognition in autism: Evidence from an fMRI study of an embedded figures task. Autism Res. 2010; 3(5):273–279. [PubMed: 20740492]

Damoiseaux JS, Rombouts SA, Barkhof F, Scheltens P, Stam CJ, Smith SM, Beckmann CF. Consistent resting-state networks across healthy subjects. Proc Natl Acad Sci U S A. 2006; 103(37):13848–13853. [PubMed: 16945915]

Desikan RS, Segonne F, Fischl B, Quinn BT, Dickerson BC, Blacker D, Buckner RL, Dale AM, Maguire RP, Hyman BT, Albert MS, Killiany RJ. An automated labeling system for subdividing the human cerebral cortex on MRI scans into gyral based regions of interest. Neuroimage. 2006; 31(3):968–980. [PubMed: 16530430]

Dong XW, Frossard P, Vandergheynst P, Nefedov N. Clustering With Multi-Layer Graphs: A Spectral Perspective. Ieee Transactions on Signal Processing. 2012; 60(11):5820–5831.

Dong XW, Frossard P, Vandergheynst P, Nefedov N. Clustering on Multi-Layer Graphs via Subspace Analysis on Grassmann Manifolds. Ieee Transactions on Signal Processing. 2014; 62(4):905–918.

Dunn OJ. Multiple comparisons among means. J Am Stat Assoc. 1961; 56:52–64.

Edgar JC, Heiken K, Chen Y, Herrington J, Chow V, Liu S, Bloy L, Huang MX, Pandey J, Cannon K, Qasmieh S, Levy SE, Schultz R, Roberts TPL. Resting-state alpha in autism spectrum disorder and alpha associations with thalamic volume. Journal of Autism and Developmental Disorders. 2014 In press.

Friman O, Farneback G, Westin CF. A Bayesian approach for stochastic white matter tractography. IEEE Trans Med Imaging. 2006; 25(8):965–978. [PubMed: 16894991]

Genovese CR, Lazar NA, Nichols T. Thresholding of statistical maps in functional neuroimaging using the false discovery rate. Neuroimage. 2002; 15(4):870–878. [PubMed: 11906227]

Ghanbari Y, Bloy L, Edgar JC, Blaskey L, Verma R, Roberts TPL. Joint Analysis of Band-Specific Functional Connectivity and Signal Complexity in Autism. Journal of Autism and Developmental Disorders. 2013

Ghanbari, Y., Smith, AR., Schultz, RT., Verma, R. Medical Image Computing and Computer Assisted Intervention (MICCAI 2013). Vol. 8149. Nagoya, Japan: Springer Berlin Heidelberg; 2013. Connectivity subnetwork learning for pathology and developmental variations; p. 90-97.

Ghanbari Y, Smith AR, Schultz RT, Verma R. Identifying group discriminative and age regressive subnetworks from DTI-based connectivity via a unified framework of non-negative matrix factorization and graph embedding. Med Image Anal. 2014

Gomot M, Belmonte M, Bullmore E, Bernard F, Baron-Cohen S. Brain hyper-reactivity to auditory novel targets in children with high-functioning autism. Brain. 2008; 131(Pt 9):2479–2488. [PubMed: 18669482]

Griffa A, Baumann PS, Thiran JP, Hagmann P. Structural connectomics in brain diseases. Neuroimage. 2013; 80:515–526. [PubMed: 23623973]

Hansen LK, Larsen J, Nielsen FA, Strother SC, Rostrup E, Savoy R, Lange N, Sidtis J, Svarer C, Paulson O. Generalizable Patterns in Neuroimaging: How Many Principal Components? NeuroImage. 1999; 9(5):534–544. [PubMed: 10329293]

Huang MX, Huang CW, Robb A, Angeles A, Nichols SL, Baker DG, Song T, Harrington DL, Theilmann RJ, Srinivasan R, Heister D, Diwakar M, Canive JM, Edgar JC, Chen YH, Ji ZW, Shen M, El-Gabalawy F, Levy M, McLay R, Webb-Murphy J, Liu TT, Drake A, Lee RR. MEG source imaging method using fast L1 minimum-norm and its applications to signals with brain noise and human resting-state source amplitude images. Neuroimage. 2014; 84:585–604. [PubMed: 24055704]

Huang MX, Nichols S, Robb A, Angeles A, Drake A, Holland M, Asmussen S, D'Andrea J, Chun W, Levy M, Cui L, Song T, Baker DG, Hammer P, McLay R, Theilmann RJ, Coimbra R, Diwakar M, Boyd C, Neff J, Liu TT, Webb-Murphy J, Farinpour R, Cheung C, Harrington DL, Heister D, Lee RR. An automatic MEG low-frequency source imaging approach for detecting injuries in mild and moderate TBI patients with blast and non-blast causes. Neuroimage. 2012; 61(4):1067–1082. [PubMed: 22542638]

Hui M, Li J, Wen X, Yao L, Long Z. An Empirical Comparison of Information-Theoretic Criteria in Estimating the Number of Independent Components of fMRI Data. PLoS one. 2011; 6:e29274. [PubMed: 22216229]

Ikemoto S. Brain reward circuitry beyond the mesolimbic dopamine system: A neurobiological theory. Neuroscience and Biobehavioral Reviews. 2010; 35(2):129–150. [PubMed: 20149820]

Ingalhalikar M, Smith A, Parker D, Satterthwaite TD, Elliott MA, Ruparel K, Hakonarson H, Gur RE, Gur RC, Verma R. Sex Differences in the Structural Connectome of the Human Brain. Proceedings of the National Academy of Sciences of the United States of America (PNAS). 2013 Published online.

Jou RJ, Jackowski AP, Papademetris X, Rajeevan N, Staib LH, Volkmar FR. Diffusion Tensor Imaging in Autism Spectrum Disorders: Preliminary Evidence of Abnormal Neural Connectivity. J Psychiatry. 2011; 45(2):153–162.

Just MA, Cherkassky VL, Keller TA, Kana RK, Minshew NJ. Functional and anatomical cortical underconnectivity in autism: evidence from an FMRI study of an executive function task and corpus callosum morphometry. Cereb Cortex. 2007; 17(4):951–961. [PubMed: 16772313]

Just MA, Cherkassky VL, Keller TA, Minshew NJ. Cortical activation and synchronization during sentence comprehension in high-functioning autism: evidence of underconnectivity. Brain. 2004; 127(Pt 8):1811–1821. [PubMed: 15215213]

Just MA, Keller TA, Malave VL, Kana RK, Varma S. Autism as a neural systems disorder: a theory of frontal-posterior underconnectivity. Neurosci Biobehav Rev. 2012; 36(4):1292–1313. [PubMed: 22353426]

Kana RK, Libero LE, Moore MS. Disrupted cortical connectivity theory as an explanatory model for autism spectrum disorders. Phys Life Rev. 2011; 8(4):410–437. [PubMed: 22018722]

Khan S, Gramfort A, Shetty NR, Kitzbichler MG, Ganesan S, Moran JM, Lee SM, Gabrieli JD, Tager-Flusberg HB, Joseph RM, Herbet MR, Hamalainen MS, Kenet T. Local and long-range functional connectivity is reduced in concert in autism spectrum disorders. Proceedings of the National Academy of Sciences of USA. 2013; 110:3107–3112.

Kim DJ, Bolbecker AR, Howell J, Rass O, Sporns O, Hetrick WP, Breier A, O'Donnell BF. Disturbed resting state EEG synchronization in bipolar disorder: A graph-theoretic analysis. Neuroimage Clin. 2013; 2:414–423. [PubMed: 24179795]

Kjaer TW, Nowak M, Lou HC. Reflective self-awareness and conscious states: PET evidence for a common midline parietofrontal core. Neuroimage. 2002; 17(2):1080–1086. [PubMed: 12377180]

Kohls G, Schulte-Ruther M, Nehrkorn B, Muller K, Fink G, Kamp-Becker I, et al. Konrad K. Reward system dysfunction in autism spectrum disorders. Social Cognitive and Affective Neuroscience. 2013; 8(5):565–572. [PubMed: 22419119]

Kohls G, Yerys B, Schultz R. Striatal Development in Autism: Repetitive Behaviors and the Reward Circuitry. Biological Psychiatry. 2014; 76(5):358–359. [PubMed: 25103541]

Lee DD, Seung HS. Learning the parts of objects by non-negative matrix factorization. Nature. 1999; 401:788–791. [PubMed: 10548103]

Leech R, Sharp DJ. The role of the posterior cingulate cortex in cognition and disease. Brain. 2014; 137(Pt 1):12–32. [PubMed: 23869106]

Liu W, Awate SP, Anderson JS, Fletcher PT. A functional network estimation method of resting-state fMRI using a hierarchical Markov random field. Neuroimage. 2014; 100:520–534. [PubMed: 24954282]

Lo YC, Soong WT, Gau SS, Wu YY, Lai MC, Yeh FC, Chiang WY, Kuo LW, Jaw FS, Tseng WY. The loss of asymmetry and reduced interhemispheric connectivity in adolescents with autism: a study using diffusion spectrum imaging tractography. Psychiatry Res. 2011; 192(1):60–66. [PubMed: 21377337]

Lou HC, Luber B, Crupain M, Keenan JP, Nowak M, Kjaer TW, Sackeim HA, Lisanby SH. Parietal cortex and representation of the mental Self. Proc Natl Acad Sci U S A. 2004; 101(17):6827–6832. [PubMed: 15096584]

Maddock RJ, Garrett AS, Buonocore MH. Remembering familiar people: the posterior cingulate cortex and autobiographical memory retrieval. Neuroscience. 2001; 104(3):667–676. [PubMed: 11440800]

Mantini D, Perrucci MG, Del Gratta C, Romani GL, Corbetta M. Electrophysiological signatures of resting state networks in the human brain. Proc Natl Acad Sci U S A. 2007; 104(32):13170–13175. [PubMed: 17670949]

Martijn, PvH, Hilleke, EHP. Exploring the brain network: A review on resting-state fMRI functional connectivity. European Neuropsychopharmacology. 2010; 20(8):519–534. [PubMed: 20471808]

Matthews PM, Filippini N, Douaud G. Brain Structural and Functional Connectivity and the Progression of Neuropathology in Alzheimer's Disease. Journal of Alzheimer's Disease. 2013; 33:S163–S172.

Montez T, Linkenkaer-Hansen K, van Dijk B, Stam C. Synchronization likelihood with explicit time-frequency priors. Neuroimage. 2006; 33(4):1117–1125. [PubMed: 17023181]

Mori S, Barker PB. Diffusion magnetic resonance imaging: its principle and applications. The Anatomical Record. 1999; 257(3):102–109. [PubMed: 10397783]

Mori S, Crain BJ, Chacko VP, van Zijl PC. Three-dimensional tracking of axonal projections in the brain by magnetic resonance imaging. Annals of Neurology. 1999; 45(2):265–269. [PubMed: 9989633]

Mori S, van Zijl PC. Fiber tracking: principles and strategies - a technical review. NMR in Biomedicine. 2002; 15(7-8):468–480. [PubMed: 12489096]

Mori S, v Zijl PCM. Fiber tracking: principles and strategies - a technical review. NMR in Biomedicine. 2002; 15(7-8):468–480. [PubMed: 12489096]

Murias M, Webb SJ, Greenson J, Dawson G. Resting state cortical connectivity reflected in EEG coherence in individuals with autism. Biol Psychiatry. 2007; 62(3):270–273. [PubMed: 17336944]

Nielsen FA, Balslev D, Hansen LK. Mining the posterior cingulate: segregation between memory and pain components. Neuroimage. 2005; 27(3):520–532. [PubMed: 15946864]

Perkins T, Stokes M, McGillivray J, Bittar R. Mirror neuron dysfunction in autism spectrum disorders. J Clin Neurosci. 2010; 17(10):1239–1243. [PubMed: 20598548]

Price G, Cercignani M, Parker GJ, Altmann DR, Barnes TR, Barker GJ, Joyce EM, Ron MA. Abnormal brain connectivity in first-episode psychosis: a diffusion MRI tractography study of the corpus callosum. Neuroimage. 2007; 35(2):458–466. [PubMed: 17275337]

Rubinov M, Sporns O. Complex network measures of brain connectivity: uses and interpretations. Neuroimage. 2010; 52(3):1059–1069. [PubMed: 19819337]

Rudie JD, Brown JA, Beck-Pancer D, Hernandez LM, Dennis EL, Thompson PM, Bookheimer SY, Dapretto M. Altered functional and structural brain network organization in autism. Neuroimage Clin. 2012; 2:79–94. [PubMed: 24179761]

Sakkalis V. Review of advanced techniques for the estimation of brain connectivity measured with EEG/MEG. Comput Biol Med. 2011; 41(12):1110–1117. [PubMed: 21794851]

Sanz-Arigita EJ, Schoonheim MM, Damoiseaux JS, Rombouts SARB, Maris E, Barkhof F, Scheltens P, Stam CJ. Loss of 'Small-World' Networks in Alzheimer's Disease: Graph Analysis of fMRI Resting-State Functional Connectivity. Plos One. 2010; 5(11)

Schipul SE, Williams DL, Keller TA, Minshew NJ, Just MA. Distinctive neural processes during learning in autism. Cereb Cortex. 2012; 22(4):937–950. [PubMed: 21725037]

Schöpf V, Windischberger C, Robinson S, Kasess CH, Fischmeister FP, Lanzenberger R, Albrecht J, Kleemann AM, Kopietz R, Wiesmann M, Moser E. Model-free fMRI group analysis using FENICA. NeuroImage. 2011; 55(1):185–193. [PubMed: 21078400]

Schultz RT, Gauthier I, Klin A, Fulbright RK, Anderson AW, Volkmar F, Skudlarski P, Lacadie C, Cohen DJ, Gore JC. Abnormal ventral temporal cortical activity during face discrimination among individuals with autism and Asperger syndrome. Arch Gen Psychiatry. 2000; 57(4):331–340. [PubMed: 10768694]

Skudlarski P, Jagannathan K, Anderson K, Stevens MC, Calhoun VD, Skudlarska BA, Pearlson G. Brain Connectivity Is Not Only Lower but Different in Schizophrenia: A Combined Anatomical and Functional Approach. Biological Psychiatry. 2010; 68(1):61–69. [PubMed: 20497901]

Sporns O, Honey CJ, Kotter R. Identification and classification of hubs in brain networks. PLoS ONE. 2007; 2(10):e1049. [PubMed: 17940613]

Sporns O, Tononi G, Edelman GM. Connectivity and complexity: the relationship between neuroanatomy and brain dynamics. Neural Netw. 2000; 13(8-9):909–922. [PubMed: 11156201]

Tang, W., Lu, Z., Dhillon, I. IEEE Int Conf Data Mining. Miami, Fl: 2009. Clustering with multiple graphs; p. 1016-1021.

van Dellen E, Hillebrand A, Douw L, Heimans JJ, Reijneveld JC, Stam CJ. Local polymorphic delta activity in cortical lesions causes global decreases in functional connectivity. Neuroimage. 2013; 83:524–532. [PubMed: 23769919]

Vissers ME, Cohen MX, Geurts HM. Brain connectivity and high functioning autism: A promising path of research that needs refined models, methodological convergence, and stronger behavioral links. Neuroscience and Biobehavioral Reviews. 2012; 36(1):604–625. [PubMed: 21963441]

Wass S. Distortions and disconnections: disrupted brain connectivity in autism. Brain Cogn. 2011; 75(1):18–28. [PubMed: 21055864]

Weng SJ, Wiggins JL, Peltier SJ, Carrasco M, Risi S, Lord C, Monk CS. Alterations of resting state functional connectivity in the default network in adolescents with autism spectrum disorders. Brain Res. 2010; 1313:202–214. [PubMed: 20004180]

Yang Z, Oja E. Linear and nonlinear projective nonnegative matrix factorization. IEEE Trans Neural Netw. 2010; 21(5):1734–1749.

Highlights

- We propose a new method for analysis of brain functional and structural connectivity networks in a population
- We identify an atlas of network hubs that describe the population and are obtained from network commonalities across the subjects
- Subject-level weights are also obtained by quantifying the intra- and inter-connectivity of network hubs that best reconstruct a subject's network
- An NMF approach combined with multi-layer graph clustering is developed to find desired network hubs
- The proposed method was applied to MEG and DTI datasets in the study of autism using modeled within- and between-hub connectivity.

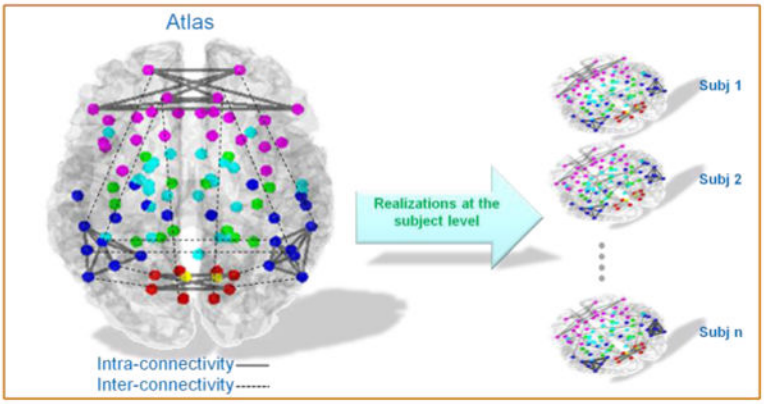

Figure 1.

The brain network is hypothesized to be made up of several hubs that are inter-connected (dashed lines), with each hub composed of a set of highly connected nodes (solid lines). The collection of hubs is considered as an atlas of connectivity. On the right, the subject-wise realizations of this network atlas show subject level variation.

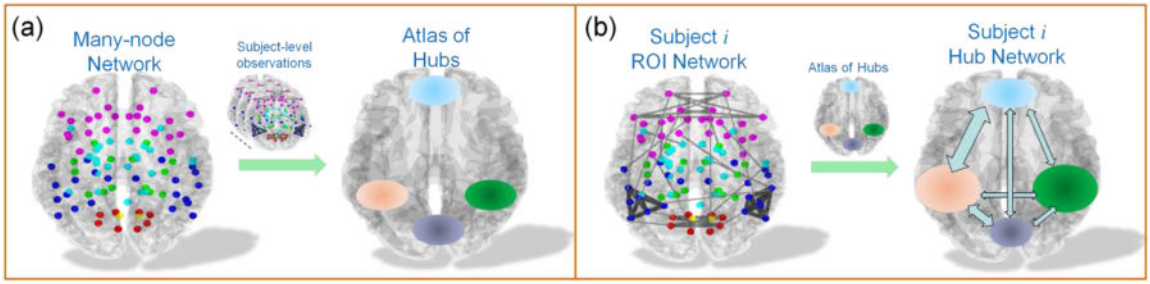

Figure 2.

Atlas of network hubs and their subject-level variation: (a) illustrates the primary objective - creating a hub atlas for a population by mapping a collection of multi-node brain networks into a system of network hubs, and (b) the second objective - given a subject's network, quantify the contribution of each network hub at the subject level (illustrated by the size of the hub) as well as the strength of the inter-connectivity between pairs of hubs in the subject's network (illustrated by the thickness of hub inter-connections)

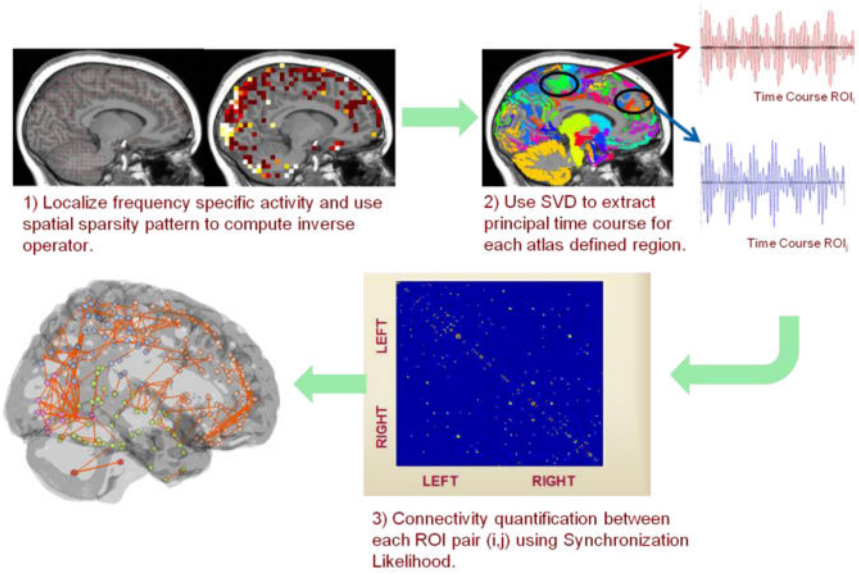

Figure 3.

Creation of functional connectome. 1) Brain activity time-series are measured on the MEG sensors and localized onto the brain regions using VESTAL in a certain frequency range. 2) Principal time courses are computed using SVD in each region. 3) Synchronization likelihood is used to quantify the functional connectivity between regions.

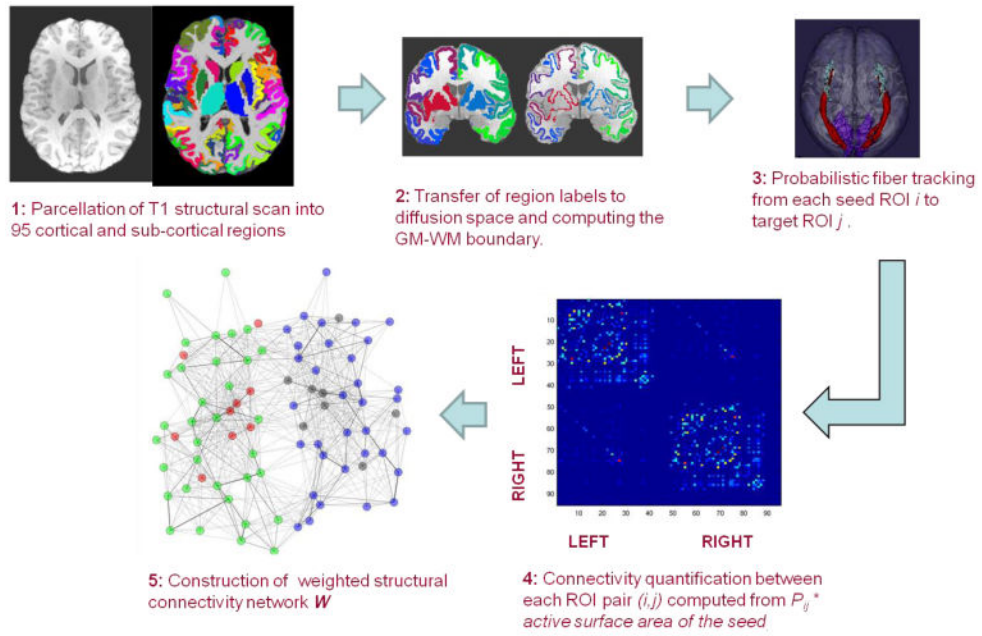

Figure 4. The pipeline in creating the structural connectome

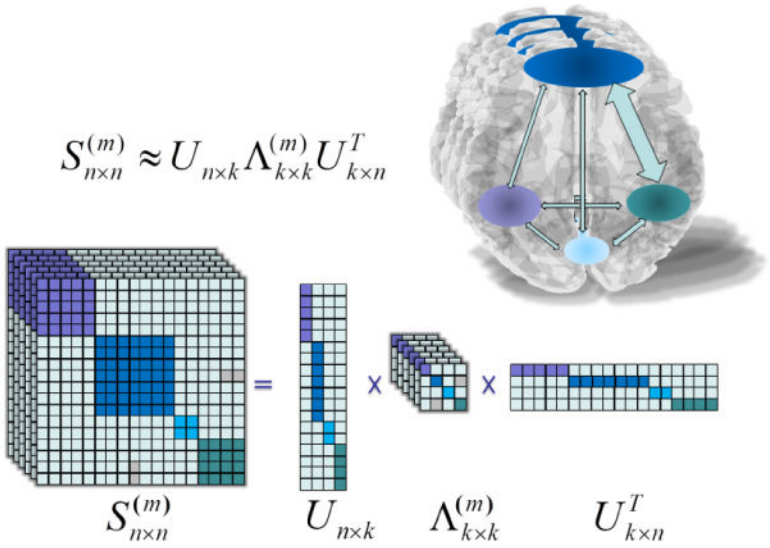

Figure 5.

The matrix decomposition of a set of connectivity matrices $\{\mathbf{S}^{(m)}\}$ forming a multi-layer graph, into a set of four network hubs as well as a set of subject-level 4×4 weight matrices. Each column of **U** characterizes the set of original nodes (ROIs) that contribute to the network hub, represented by the same-color ellipse on the brain map. The elements of $\mathbf{\Lambda}^{(m)}$ also describe the strength of intra- and inter-connectivity of network hubs.

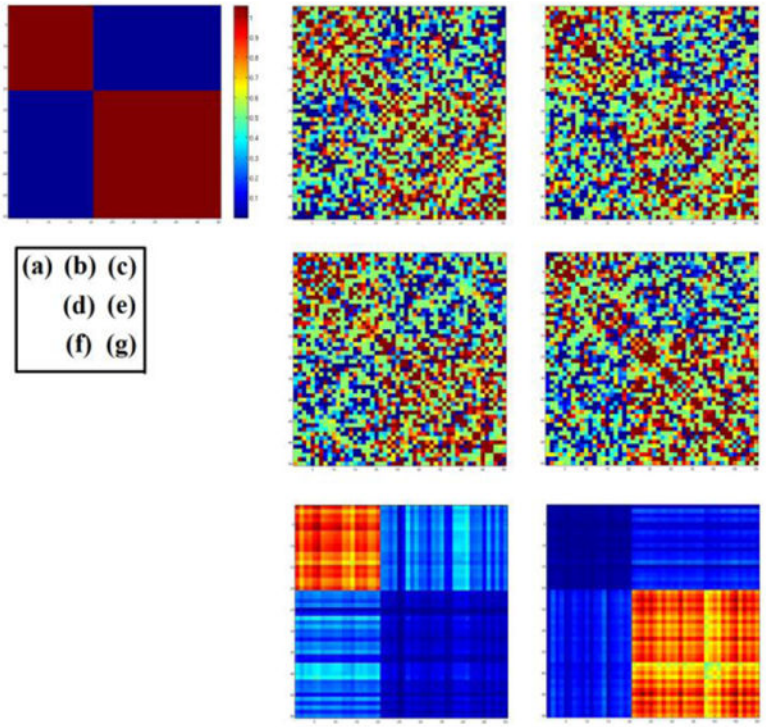

Figure 6.

The simulation of four networks as variations of an underlying network with two hubs, and the hubs obtained from the proposed method. (a) the connectivity matrix of a network consisting of two hubs. (b)-(d) the simulated subject-level variations of the original network. (f)-(g) show the resulting two hubs obtained from the proposed algorithm. Blue is smallest and red is highest values in the images.

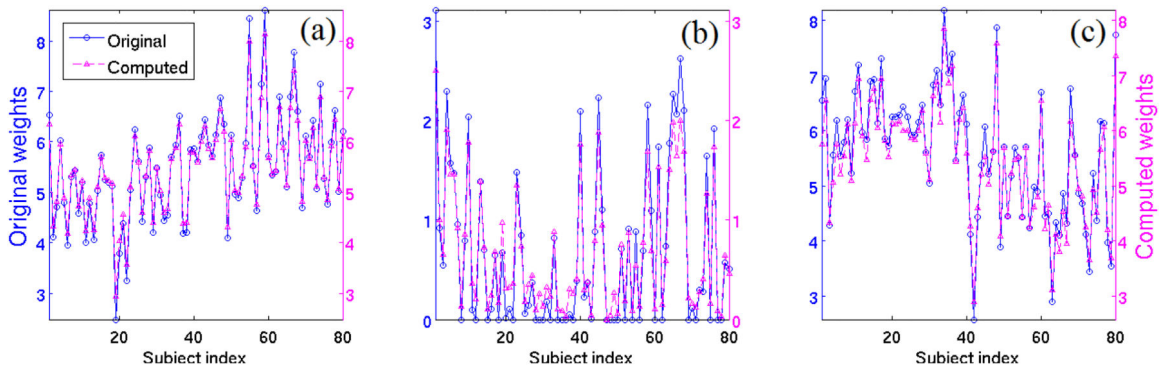

Figure 7.

The original and rescaled computed weights of 80 networks constructed from randomized weights over two fixed hubs of Fig 6(a). (a) Intra-connectivity weights of hub 1. (b) Inter-connectivity weights between hub 1 and hub 2. (c) Intra-connectivity weights of hub 2.

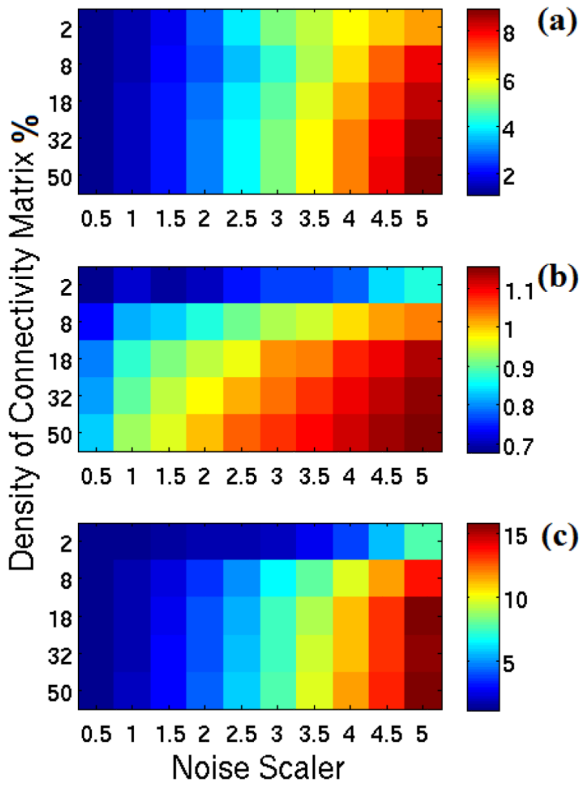

Figure 8.

The mean squared error (MSE) of the computed weights when connectivity density and noise variance change. Horizontal axis includes the coefficients that scale the standard deviation of the background noise as well as the group-wise noise in weights. Vertical axis is the density of the underlying connectivity in percent. MSEs are color-coded for the computed (a) intra-connectivity of hub1, (b) inter-connectivity weights between hub 1 and hub 2, (c) intra-connectivity weights of hub 2.

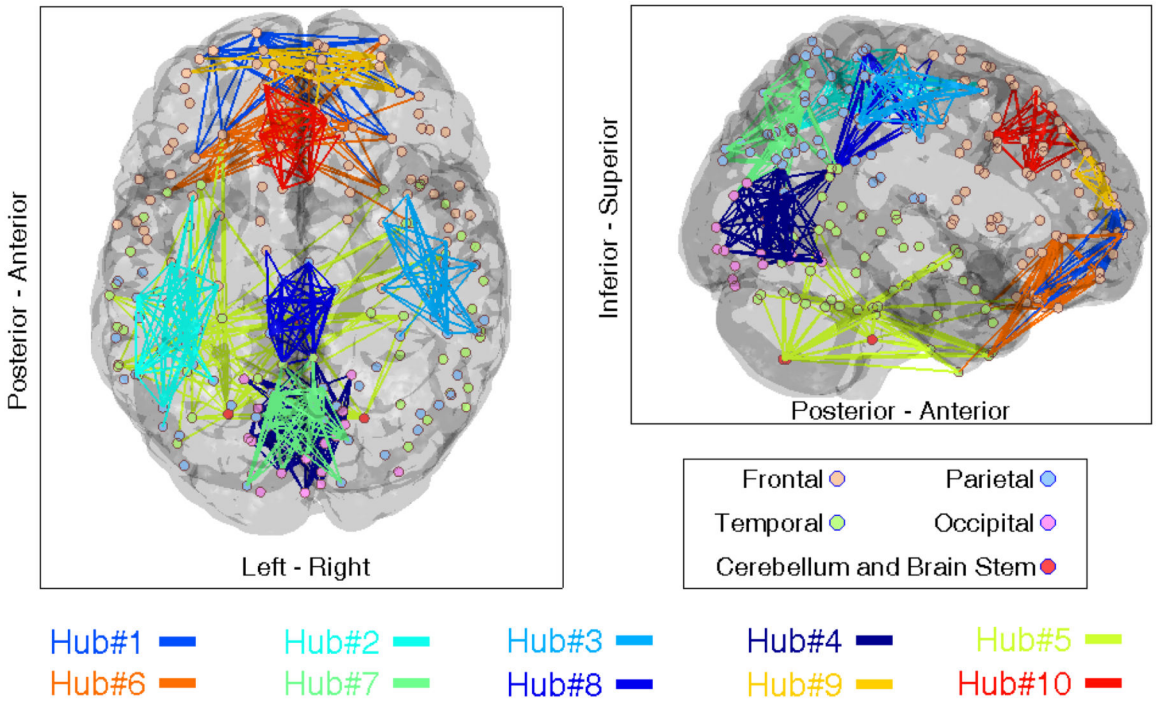

Figure 9.

The *k*=10 functional connectivity network hubs of alpha activity obtained from the ASD + TDC subjects. Hubs are displayed (in no specific order) on a brain map with 202 ROIs. Each hub is given a color shown by the connections between regions. Each ROI is also color-coded by the brain lobe (frontal, temporal, parietal, occipital, Cerebellum and Brain Stem).

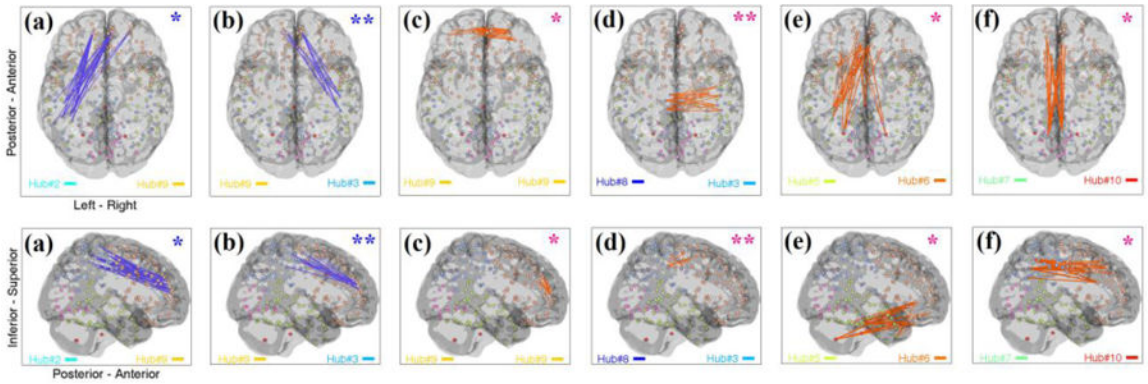

Figure 10.

The intra- and inter-connectivity group difference patterns (axial view in top panels and sagittal view in bottom panels). Blue and orange networks have higher weights in TDC and ASD, respectively. Components with group weight difference of $p<0.05$ are labeled with one star (on the top right of each panel), and weight differences of $p<0.01$ with two stars. Each sub-network is also labeled with the corresponding hubs (shown at the bottom of each panel with their color-coded names as in Fig. 9) whose intra- or inter-connectivity forms that pattern.

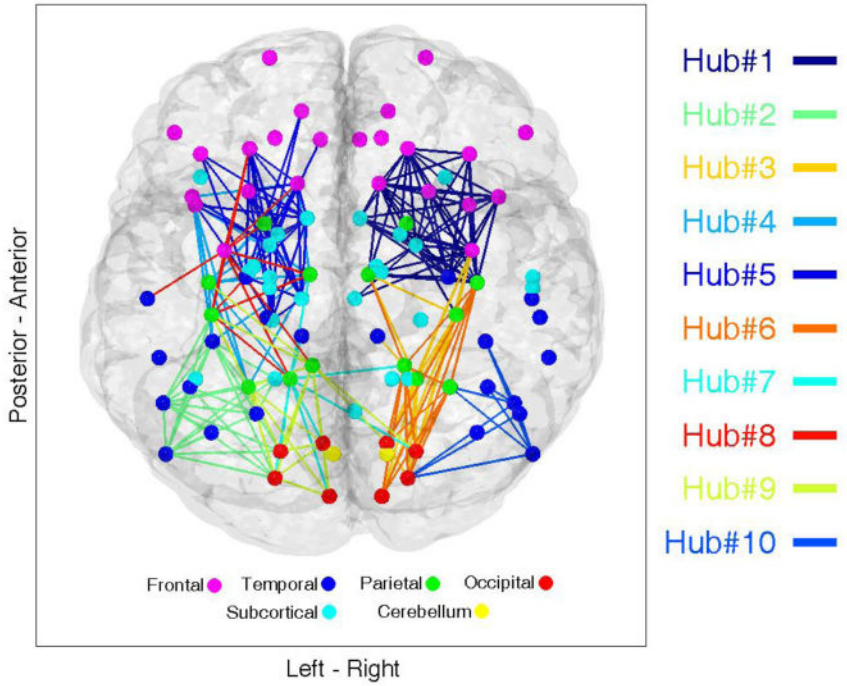

Figure 11.

The 10 network hubs obtained from the pool of connectivity matrices of the 198 subjects, displayed in no specific order on the brain map with 95 ROIs. Each ROI is color coded with its brain lobe, and each hub is color-coded with a given numbered name.

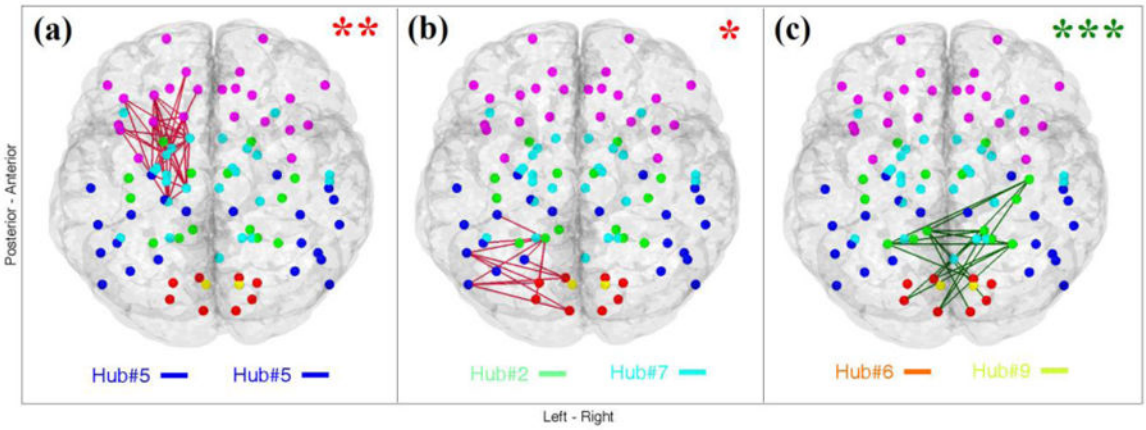

Figure 12.

The intra- and inter-connectivity patterns that show significant differences between ASD and TDCs. Red and green connection lines, respectively, indicates decreased and increased weights in ASD versus TDC. Specifically, (a) the intra-connectivity pattern of network hub #5 (blue in Fig. 11) with weights decreased in ASD with $p<0.01$, (b) the inter-connectivity pattern between hub #2 (green in Fig. 11) and hub #7 (cyan in Fig. 11) with weights decreased in ASD with $p<0.05$, (c) the inter-connectivity between hub #6 (orange in Fig. 11) and hub #9 (lemon in Fig. 11) with increased weights in ASD with $p<0.005$. The color of nodes indicates their lobe as coded in in Fig. 11.

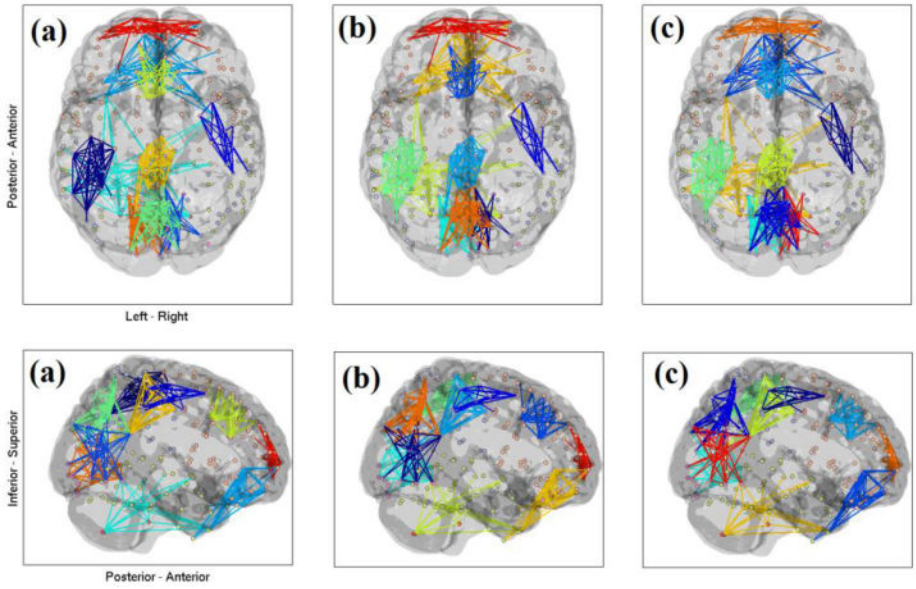

Figure 13.

The *k*=10 functional connectivity network hubs of alpha activity obtained from the TDC subjects when regularization parameter varies. (a)-(c) demonstrate the hubs obtained from 40 TDC subjects when the regularization parameter was set to β=0.01, 0.1, and 0.2, respectively. The colors are randomly assigned to hubs in each panel.

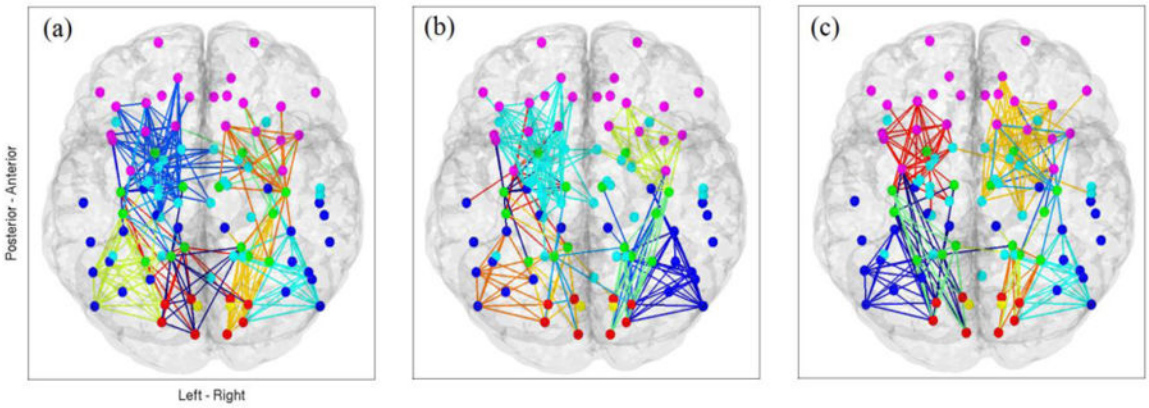

Figure 14.

The *k*=10 structural connectivity network hubs obtained from the TDC subjects when regularization parameter varies. (a)-(c) demonstrate the hubs obtained from 82 TDC subjects when the regularization parameter was set to β=0.01, 0.1, and 1, respectively. The colors are randomly assigned to hubs in each panel.

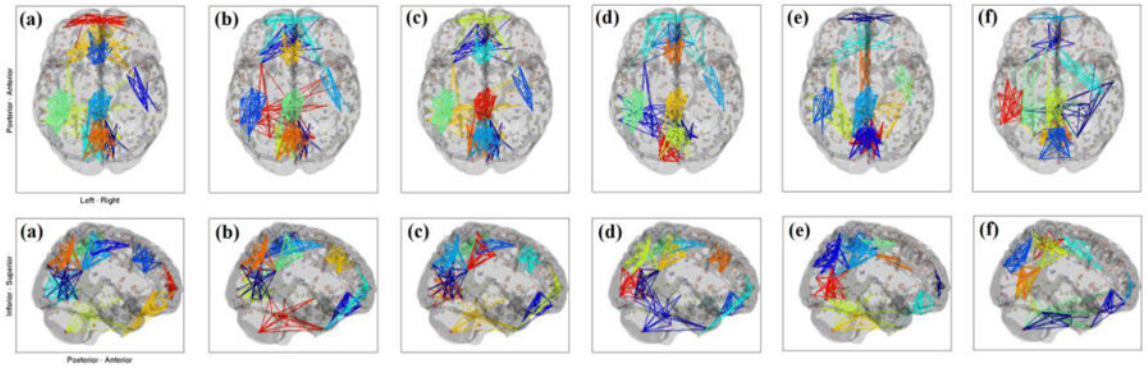

Figure 15.

The k=10 functional connectivity network hubs of alpha activity obtained from the TDC subjects. (a)-(f) show the hubs obtained from 40, 37, 34, 25, 15, and 5 TDC subjects, respectively. The colors are randomly assigned to hubs in each panel.

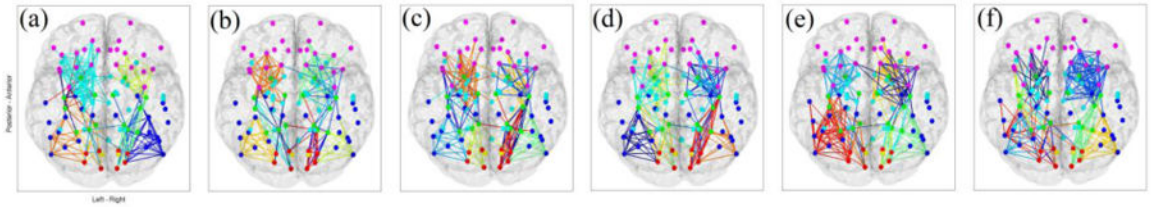

Figure 16.

The *k*=10 structural connectivity network hubs obtained from the TDC subjects. (a)-(f) show the hubs obtained from 82, 60, 40, 20, 10, and 5 TDC subjects, respectively. The colors are randomly assigned to hubs in each panel.

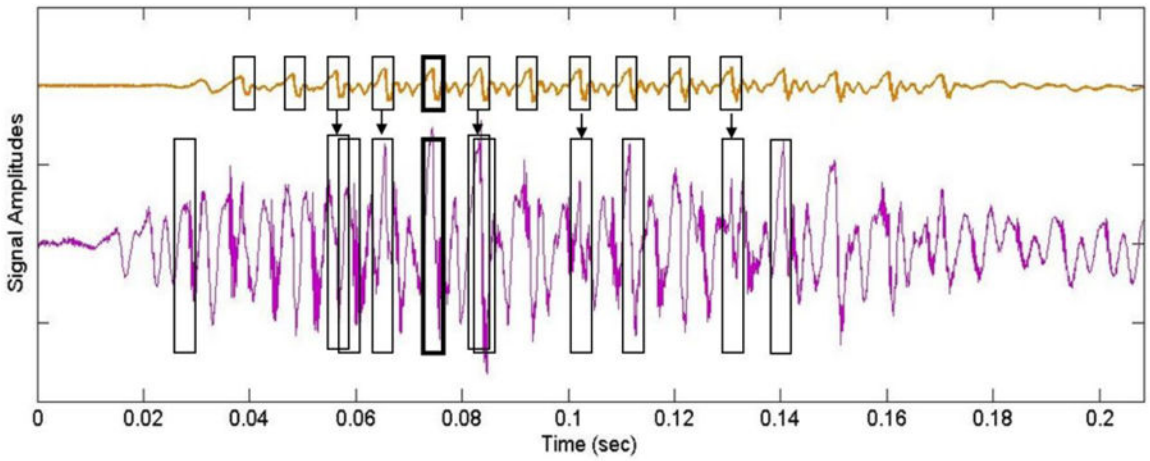

Figure 17.

The intra An illustration of synchronization likelihood between two signals from two channels plotted by different colors. A reference pattern was selected at the time 0.074 sec (thick rectangle). The recurrences in both signals are shown by thin rectangles for *nref* = 10. Vertical arrows show simultaneous recurrences in both channels. SL at time 0.074 is therefore equal to the ratio between number of simultaneous recurrences and the number of *nref*, i.e. SL = 5/10 = 0.5.

Table 1

The group-wise t-values for the original and computed weights when the parameter beta changes.

	t_{11} (intra-connectivity of hub 1)		t_{12} (inter-connectivity between hubs 1 and 2)		t_{22} (intra-connectivity of hub 2)	
	Original	**Computed**	**Original**	**Computed**	**Original**	**Computed**
$\beta = 0.01$	-4.1	-4.1	+0.5	+1.2	+3.6	+3.3
$\beta = 0.1$	-4.9	-4.9	-0.8	-0.1	+6.1	+6.0
$\beta = 1$	-4.9	-4.9	+0.5	+1.1	+3.6	+3.5

Table 2

The top ranked anatomical regions according to their membership in the network hubs (Fig. 9).

Hub #1	Superior frontal (left and right), Rostral middle frontal (left and right), Lateral orbito frontal (right and left)
Hub #2	Superior parietal (left), Supermarginal (left), Pre and post central (left)
Hub #3	Pre and postcentral (right), Supramarginal (right), Caudal middle frontal (right)
Hub #4	Pericalcarine (right and left), Lingual (right and left), Precuneus (right and left)
Hub #5	Fusiform (left and right), Cerebellum (left and right) and brain stem, Parahippocampal (left)
Hub #6	Medial orbito frontal (left and right), Rostal anterior cingulate (left and right), Lateral orbito frontal (left and right)
Hub #7	Precuneus (left and right), Superior Parietal (left and right)
Hub #8	Posterior cingulate (left and right), Paracentral (left and right), Isthmus cingulate (left and right)
Hub #9	Superior frontal (right and left), Rostral middle frontal (right and left), superior frontal (right and left)
Hub #10	Caudal anterior cingulate (right and left), Superior frontal (right and left)

Table 3

The significant developmental differences between ASD and TDC obtained by a GLM model with group, age and their interaction as predictors ($p<0.05$).

Hubs	**Group-wise correlation between age and the hub weights**		**The primary ROIs**
	ASD	**TDC**	
Hub 5 and hub 8 inter-connectivity	-0.26	+0.28	connections of left fusiform and cerebellum with left posterior cingulate and paracenral regions
Hub 10 intra-connectivity	-0.29	+035	connections between caudal anterior cingulate and superior frontal regions

Table 4

The top ranked anatomical regions according to their membership to the network structural Fig. 11.

Hub #1	Precentral (right), Putamen (right), Superior frontal (right)
Hub #2	Middle Temporal (left), Inferior temporal (left), Fusiform (left)
Hub #3	Superior parietal (right), Supramarginal (right), Precentral (right)
Hub #4	Postcentral (left), Caudal middle frontal (left), Paracentral (left)
Hub #5	Putamen (left), Insula (left), Caudate (left)
Hub #6	Precuneus (right), Inferior parietal (right), postcentral (right)
Hub #7	Superior parietal (left), Cuneus (left), Lingual (left)
Hub #8	Precentral (left), Supramarginal (left), Superior Parietal (left)
Hub #9	Precuneus (left), Inferior Parietal (left), Cuneus (left)
Hub #10	Inferior temporal (right), Middle temporal (right), Fusiform (right)